Mine Water and the Environment (2023) 42:418–440
https://doi.org/10.1007/s10230-023-00946-2

TECHNICAL ARTICLE

Hydro-Mechanically Coupled Numerical Modelling of Protective Water Barrier Pillars in Underground Coal Mines in India

Ankush Galav[1] · G. S. P. Singh[1] · S. K. Sharma[1]

Received: 8 December 2022 / Accepted: 27 July 2023 / Published online: 16 August 2023

Abstract
Protective water barrier pillars (PWBPs) are inter-mine barrier pillars. An adequate PWBP can protect active mine workings from the danger of inundation from adjoining inundated workings. This paper discusses a hydro-mechanical coupled numerical modeling approach for the design of PWBPs, considering different flow regimes. The coupled model considers the effect of seepage through the roof, pillar, and floor on the mechanical strength of the rock mass and vice-versa. A statistical model based on the extent of positive volumetric strain zones (ZoPVS, %) was formulated to assess the mechanical stability of the pillar. The model considers the pillar width, cover depth, strength, modulus of elasticity of coal and roof/floor, and the extraction ratio as the input parameters. Based on the results of numerical modeling-based parametric studies, statistical models were developed to estimate the seepage rate for assessing the hydraulic performance of the pillar. The seepage rate of water through a PWBP was estimated in terms of the cover depth of the seam, compressive and tensile strengths and modulus of elasticity of the pillar system, mean in-situ horizontal stress, pillar width, extraction ratio, and permeability of the rock mass. A ZoPVS of 95% represented unstable behavior and piping failure of the pillar. The maximum seepage rate of 315 L/s/km (5000 GPM/km) was reckoned as the acceptable hydraulic performance of the PWBP based on the field experience in Indian geo-mining conditions. The validation of the model for two case studies with minimum pillar widths of 30–60 m at a cover depth of 84.5–134.5 m was in agreement with the field experiences.

Keywords Inundation · Pillar design · Seepage · Hydro-mechanical coupled modeling · Numerical simulation

Introduction

Protective water barrier pillars (PWBPs) are designed to protect active mine workings from the danger of accidental inrush of water from old, inundated workings. Such uncontrolled seepage of water can endanger the lives of miners and cause the loss of minerals and machinery underground. Improper surveying and incompetent barrier dimensions have been identified as the primary reasons for these disasters (Dash et al. 2016; Galav et al. 2021; Job 1987).

The stability of PWBPs is governed by the mechanical and hydraulic properties of the rock mass. Hence, the stability of such pillars results from the hydro-mechanical interaction of influencing parameters, which includes pillar dimension, cover depth, extraction ratio, the compressive and tensile strengths of rock mass, and the modulus of elasticity (Table 1), state of stresses, permeability, and water head (Galav et al. 2021; Kendorski and Bunnell 2007). In the last two centuries, several attempts have been made to formulate a practical design approach for a PWBP. However, most of these approaches are now obsolete as they grossly ignored the influence of the most important mechanical and hydraulic parameters.

Various approaches have evolved based on trial and error, field study, laboratory study, numerical simulation, empirical design, etc. (Chen et al. 2017; Galav et al. 2021, 2022; Kendorski and Bunnell 2007; Kesserü 1982; Luo et al. 2001; Meng et al. 2016; Singh and Atkins 1982; Yang et al. 2007; Wang et al. 2019; Zhang and Li 2022; Zhao et al. 2021; Zhu et al. 2015). Numerical simulation, in combination with others, is the most effective design tool with proper inputs and validation to explore the full spectrum of the problem. In the last few decades, many attempts have been made to understand the interaction of mechanical parameters, such as stress and strain, on hydraulic parameters (porosity, permeability,

✉ G. S. P. Singh
gspsingh.min@itbhu.ac.in

[1] Department of Mining Engineering, IIT(BHU), Varanasi 221005, India

Table 1 Existing design approaches and their description (Kendorski and Bunnell 2007; DGMS 2017; Galav et al. 2021)

	Name	Pillar Width, m	Description
1	Dunn's Rule	$\frac{(D-54.86)}{20} + 4.57$	It suggested a 4.57 m wide barrier for a cover depth of 54.86 m to be increased by 0.91 m for every 18.29 m of increase in cover depth, obsolete now due to undersized pillar estimation
2	Ashley's Method or Pennsylvania Mine Inspector's Equation	$\frac{D}{10} + 4h + 6.1$	D is the water head if it is greater than the cover depth; a potential relationship that considers the depth, seam thickness, and water head
3	Ash and Eaton's Impoundment Equation	$\frac{D}{2.35} + 15.24$	Did not consider the strength and hydraulic properties
4	Outcrop Water Barrier Pillars	$\frac{D}{3.28} + 15.24$	Developed after several failures of undersized PWBP against large water heads in Kentucky, USA, the effect of the strength was not considered
5	Old English Barrier Pillar Law	$\frac{Hh}{30.48} + 5h$	Not recommended for dry barrier pillars and extraction height greater than 4.57 m; strength not considered
6	The Pressure Arch Method	$2.625 * \left(\frac{D}{20} + 6.1\right)$	Considers the effect of load redistribution, suggested for a cover depth of 122–853 m, does not consider the strength and hydraulic properties
7	British Coal Rule of Thumb	$\frac{D}{10} + 13.72$	used in British mines, does not consider the strength and hydraulic properties
8	Coal Mine Regulation of India 2017	60	Not a scientific design approach and does not consider any mechanical or hydraulic parameter

(D is cover depth, h is extraction height, and H is water head, all in m)

etc.) (Durucan 1981; Esterhuizen and Karacan 2007; Galav et al. 2021; Prusty et al. 2015; Whittles et al. 2006; Zhang and Wang 2006). These attempts need to be explored further for an improved understanding of the subject.

Galav et al. (2021) provided guidelines for the design of a PWBP and highlighted the mechanics involved, most influential parameters, existing design criteria, associated challenges, and knowledge gaps in the design of PWBP in light of the disasters caused due to inundation worldwide. In a subsequent communication (Galav et al. 2022), only the study of hydro-mechanical stability of the PWBP for seepage through the pillar was reported. A significant increase in the rate of water seepage was noted for the zone of failure (ZoF), exceeding 70% of the total number of zones in the pillar, followed by an exponentially increasing trend for the failure zones exceeding 95%, indicating its unstable behavior. Although this design criterion successfully explained the performance of a PWBP at moderate cover depth, it could not capture the seepage characteristics at shallow-depth workings. Further, in practice, flow through the 'pillar only' is low compared to other flow paths. Much of the seepage in most of the mines flows through their roof and floor, which are often composed of sandstone. Field observation revealed a great deal of seepage in these workings, which necessitated an extension of the study to understand the hydro-mechanical behavior of the different flow regimes.

This paper discusses the findings of further study considering the effect of flow through the roof and floor in addition to flow through the pillar, obtaining an improved design criterion for its large-scale application. The hydro-mechanical coupled numerical modelling approach forms the major novelty of this work. The ZoF-based criterion was replaced by the extent of positive volumetric strain zones (ZoPVS) for improved evaluation of the mechanical performance of the pillar. The positive volumetric strain zones (ZoPVS, %) were used to assess the mechanical stability, while the seepage rate was used to assess the hydraulic performance of the pillars. A ZoPVS of 95% indicated an inadequately designed pillar at a cover depth of 100–350 m. The strain softening behavior for different sizes of pillars and back estimation of their governing parameters are discussed along with the predictive relationship of the ZoPVS and the seepage rate for different conditions. A maximum seepage of 315 L/s/km (5000 GPM/km) was reckoned for controlled seepage through the pillar.

Design Consideration

The adequacy of a PWBP is governed by its mechanical and hydraulic performance. Mechanical failure of the pillar is stress governed, whereas its hydraulic failure is strain-governed. The in-situ porosity and permeability that affect the seepage are modified by strain-controlled fracturing. As the pillars get loaded by the redistributed stresses due to excavation, they get divided into slumped, crushed, yielded, and intact sub-domains in sequence toward the center (Galav et al. 2021). The extent of slumped, crushed, and yielded zones defines the extent of damage in the pillar. With an increased extraction ratio, the pillar stress intensifies, and the extent of the damage increases. An equivalent change is induced in the hydraulic properties of the rock matrix with the amount of damage, as manifested by an increased rate of water seepage. The damage also affects

the hydro-mechanical response of the barrier pillars. The resistance to seepage from the barrier pillars is reduced with an increase in the width of the damage zone and a decrease in the width of the intact zone.

Flow through the overburden, mine floor, and PWBP are the primary sources of water in the mines facing significant seepage. Generally, the seepage per unit area through an intact barrier pillar is slow, steady, and laminar. It follows Darcy's law (Eq. 1) and is governed by the intrinsic permeability (k), dynamic fluid viscosity (μ), fluid pressure difference among the domains (ΔP), and flow length (l).

$$Q = -\frac{k}{\mu}\frac{\Delta P}{l} \tag{1}$$

The overburden seepage in an underground mine can be calculated using Eq. 2 (Ministry of Water Resources, government of India 2009; Soni 2019).

$$\mathrm{Q}_{mos} = \frac{L_A R_a C_{RIF}}{M_A} \tag{2}$$

where Q_{mos} is the maximum feasible overburden seepage in m^3/annum, L_A is the lease area in m^2, M_A is the mined area in m^2, R_a is the average rainfall in m^3/annum, and C_{RIF} is the rainfall infiltration factor (0.05–0.07).

Table 2 shows the field data compiled from different underground coal mines in India, reflecting the conditions of existing PWBPs. The width of the barrier pillars ranged from 10–650 m at a cover depth of 18–300 m with a water head of 10–207 m and seepage ranging from negligible to 265 L/s (4200 GPM). The previous study revealed that there was very little correlation between the depth of cover and the width of the PWBP (Galav et al. 2022). High seepage was experienced in almost 50% of the cases where the prevailing width was less than the minimum regulatory limit (60 m). There is an urgent need to assess the stability of the PWBPs and establish effective measures for mitigating the danger of inundation in all such cases. Pillars that were at least 200 m wide at a cover depth of 18–91 m and 650 m wide at a cover depth of 78–164 m did not experience significant seepage. However, a large amount of coal is locked up in such a barrier. Hence, the design of a PWBP should be based on scientific considerations, especially the safety and techno-economics of the structure.

Numerical Modelling

The flowchart shown in Fig. 1 was followed for numerical modeling of a PWBP using the finite difference software FLAC 2D (ITASCA 2011). The modeled pillar system (Fig. 2) consisted of a 3 m thick coal seam sandwiched between a 50 m thick floor and roof and the interfaces in between. The width of the model varied according to the pillar and gallery widths. A fixed gallery width of 5 m was considered in all cases. The model geometry was discretized using 0.5 × 0.5 m size elements.

In situ vertical stress corresponding to the remaining depth of cover was applied on the upper boundary based on Eq. 3, while the mean horizontal stress estimated using Eq. 4 (Sheorey 1994) was initialized in the model.

$$\sigma_v = \gamma D \tag{3}$$

$$\sigma_h = \frac{\vartheta}{1-\vartheta}\gamma \mathrm{D} + \frac{\beta \mathrm{EG}}{1-\vartheta}(\mathrm{D} + 1000) \tag{4}$$

where σ_v is the vertical stress in MPa, σ_h is the mean horizontal stress in MPa, γ is the unit weight of rock in MPa/m, ϑ is Poisson's ratio, D is the cover depth in m, β is the thermal expansion coefficient of rock, E is the modulus of elasticity in GPa, and G is the geothermal gradient of strata.

The parametric study considered the possibilities of seepage through the coal seam, floor, roof, and their combinations to analyze the induced permeability and corresponding flow patterns for varying working depth, pillar width, percentage of extraction, water head, porosity, permeability, and rock-mass strength. These results were used to analyze the hydro-mechanical performance of the pillars under different geomining conditions. The study considered variations in the flow regime as flow through pillar only, roof only, floor only, pillar and roof/floor, and the pillar system (i.e. roof, pillar, and floor). For each flow regime, the study incorporated variations in working depths from 100 to 350 m, pillar widths from 15 to 120 m, percentages of extraction from 10 to 44%, water head from 25 to 100% of cover depth, coal permeability from 2.97×10^{-13} to 9.90×10^{-11} m^2/Pa·s, permeability of roof and floor ranging from 9.90×10^{-12} to 9.90×10^{-10} m^2/Pa·s and the rock mass strength properties given in Table 3. These strength properties were classified into three categories: soft, average, and hard, based on the conditions prevailing in different coalfields in India (Singh 2007). The height of the developed pillar was not changed in the parametric study since it did not vary significantly in the reference database.

The friction angle for coal was taken as 25° and 40° for other rock masses, based on experience. The dilation angle was fixed at 5° for the other rock mass, whereas the initial dilation angle value was considered zero for coal. The Poison's ratio of 0.25 was considered for coal and 0.35 for other rocks. The shear modulus (G), bulk modulus (B), and cohesion (C) were calculated using Eq. 5–7, respectively. A roller boundary condition was applied on the vertical boundary at the two sides and a rigid boundary to the model floor (Fig. 2).

Table 2 Geo-mining condition along with the operational condition of PWBP in Indian coal mines

Sl. No	Mine_ Adjacent Mine / Working Seam_ Working Seam	Depth, m	Width, m	Water Head, m	Seepage, L/s
1	Sonepur Bazari_RVIII Seam	18	200	18	Negligible
2	Siduli_RVIII Seam	25	110	25	Negligible
3	Mahamaya UG Mine_Mahan OCM	27	125	100	38
4	Dhelwadih UG Mine_	58	25	115	139
5	Mahusudhanpur 7Pit & Incline_Khas Kajora Colliery	59	60	59	Negligible
6	Sonepur Bazari_RVII Seam	71	200	71	Negligible
7	Porascole (west) Colliery_CL Jambad Colliery	72	26	72	32
8	Bankola_RVIII Seam	78	60	78	Negligible
9	Khandra_RVIII Seam	78	650	78	Negligible
10	Singhali_	80	25	80	221
11	Sonepur Bazari_RVIIA Seam	91	200	91	Negligible
12	Patmohana Colliery _East: Dhemomain Incline_RVIII Seam	92	45	92	221
13	Madhabpur Colliery_East: Naba Kajora Colliery	93	10	93	Not Available
14	Madhabpur Colliery_West: Parasea 6&7 Incline	93	20	93	Not Available
15	Madhabpur Colliery_North: Nabakajora Colliery	93	60	93	Negligible
16	Madhabpur Colliery_South: Lachipur Colliery	93	60	93	Negligible
17	Siduli_RVII Seam	101	62	101	Negligible
18	Central Kajora Colliery_Lachipur Colliery, Ghanshyam Colliery, Madujore Colliery	104.5	15	104.5	Not Available
19	Gayatri UG mine_ Rehar UG Mine	106.5	43	106.5	221
20	Patmohana Colliery _West: Chinakuri Colliery-III_R-VIII Seam	109	40	109	63
21	Nabakajora Colliery_Lachipur Colliery	110.5	15	110.5	Not Available
22	Siduli_RVIIA Seam	119	180	119	Negligible
23	Rajnagar RO_Handidhua UG Mine	120	50	13	2000
24	Naba Jambad Project_CL Jambad Colliery	120	11.5	110	Not Available
25	Rajgamar 4&5 Incline_North: Rajgamar 6&7	125	120	15	126
26	Rajgamar 4&5 Incline_South: Pawan Incline	130	60	32	189
27	Bagdeva_G-III Bottom Seam	136	22	24	51
28	Bankola_RVII Seam	140	50	140	Negligible
29	Khandra_RVII Seam	140	650	140	Negligible
30	Dhemomain (Pit) Colliery_North: R.B. Seam_ R-VA Seam	150	180	150	13
31	Porascole (East) Colliery_Madhusudanpur 3&4 Pit & PSC (E)__Kajora_RIX Seam	159.5	26	159.5	46
32	Bankola_RVIIA Seam	164	50	164	Negligible
33	Khandra_Khandra_ RVIIA Seam	164	650	164	Negligible
34	Rajnagar RO_4A Seam	167	20	67	265
35	Rajnagar RO_Hingir Rampur Colliery UG Mine	175	42	141	152
36	Jamabad UG Colliery_	200	17.5	200	Not Available
37	Porascole (East) Colliery_Moila & PSC (E) Colliery_Jambad_ RVIII Seam	207	16	207	22
38	Porascole (East) Colliery_Madhusudanpur 3&4 Pit & PSC (E)__Jambad_RVIII Seam	207	13.5	207	46
39	Parbelia Colliery (Incline)_Hijuli_RVIII Seam	212		10	7
40	Chinakuri Mine- III_Patmohana Colliery	300	60	105	7

$$G = \frac{E}{2(1+\vartheta)} \tag{5}$$

$$B = \frac{E}{3(1-3\vartheta)} \tag{6}$$

$$C = \frac{\sigma_c}{2\tan\left(\frac{\pi}{180}\left(\frac{\Phi}{2}+45\right)\right)} \tag{7}$$

where E is the modulus of elasticity, ϑ is Poisson's ratio, σ_c is compressive strength, and Φ is the angle of internal friction.

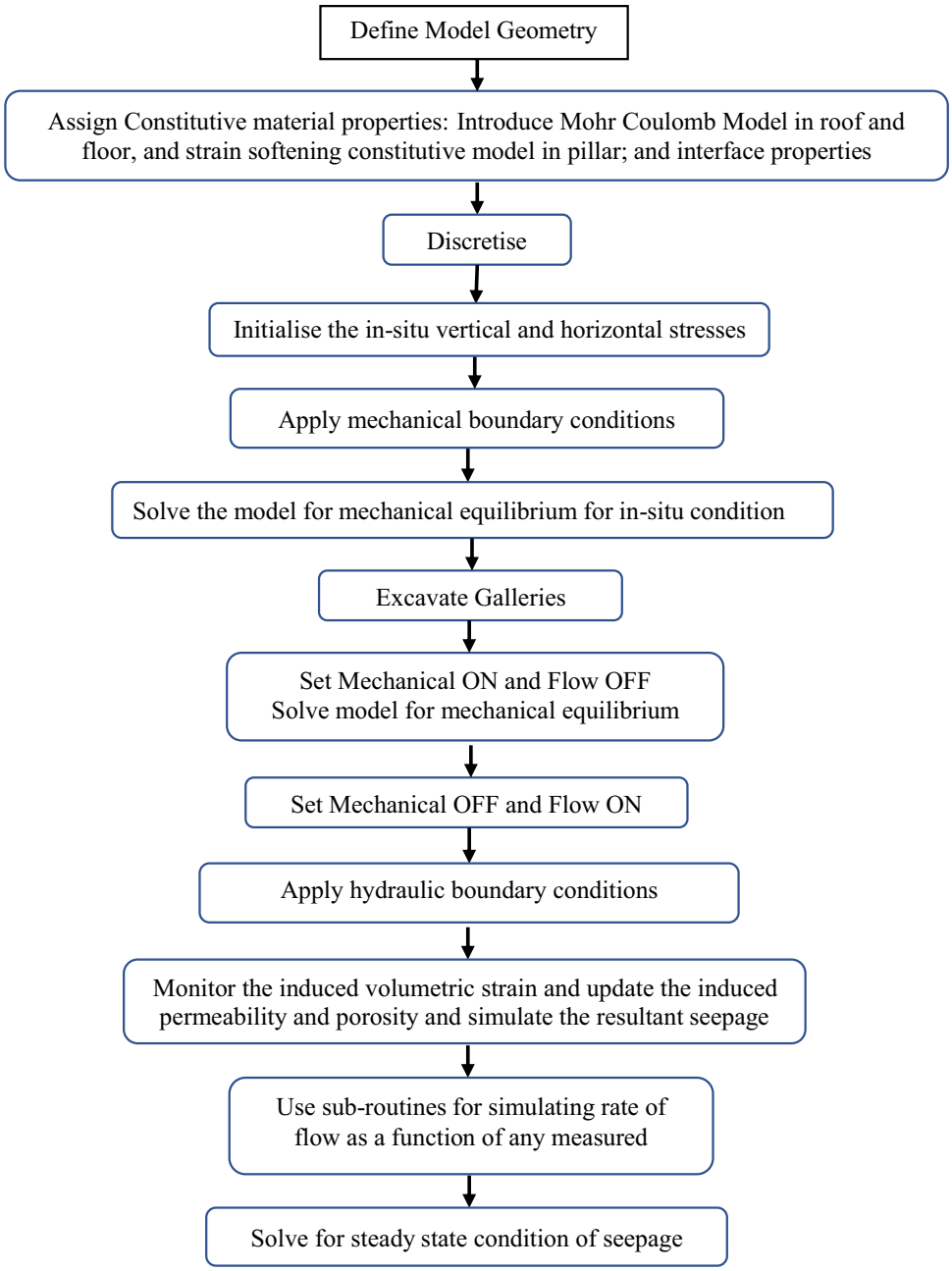

Fig. 1 Methodology of numerical simulation for the mechanical-hydraulic coupled modeling of Protective Water Barrier Pillars

The mobility coefficient and porosity are the critical parameters for the modeling of seepage in FLAC. The mobility coefficient is defined as the ratio of the permeability of the rock mass and the dynamic viscosity of the fluid. Equation 8 (ITASCA 2011) was used for updating the induced porosity as a function of the induced volumetric strain in the model. Similarly, the mobility coefficient was updated using Eq. 9 (Zhu et al. 2015).

$$n = 1 - \frac{1 - n_o}{1 + e_v} \tag{8}$$

$$k = k_o\left[\left\{\left(\frac{1}{n_o}\right)\left(1 + e_v\right)^3\right\} - \left\{\left(\frac{1 - n_o}{n_o}\right)\left(1 + e_v\right)^{-1/3}\right\}\right]^3 \tag{9}$$

where k is the induced mobility coefficient in m^2/Pa·s, n is the induced porosity, n_o is the insitu porosity, e_v is the induced volumetric strain, and k_o is the insitu mobility coefficient in m^2/Pa·s.

A sensitivity analysis (Lönnies 2017) revealed that interface properties greatly affect the characteristic behavior of pillars. Considering several approaches, including the FLAC manual (ITASCA 2011), and Lonnies (2017),

the interface properties given in Table 4 were used for this study.

Cylindrical coal samples 54 mm in diameter with width/height (w/h) ratios of 0.5–10 were laboratory tested using

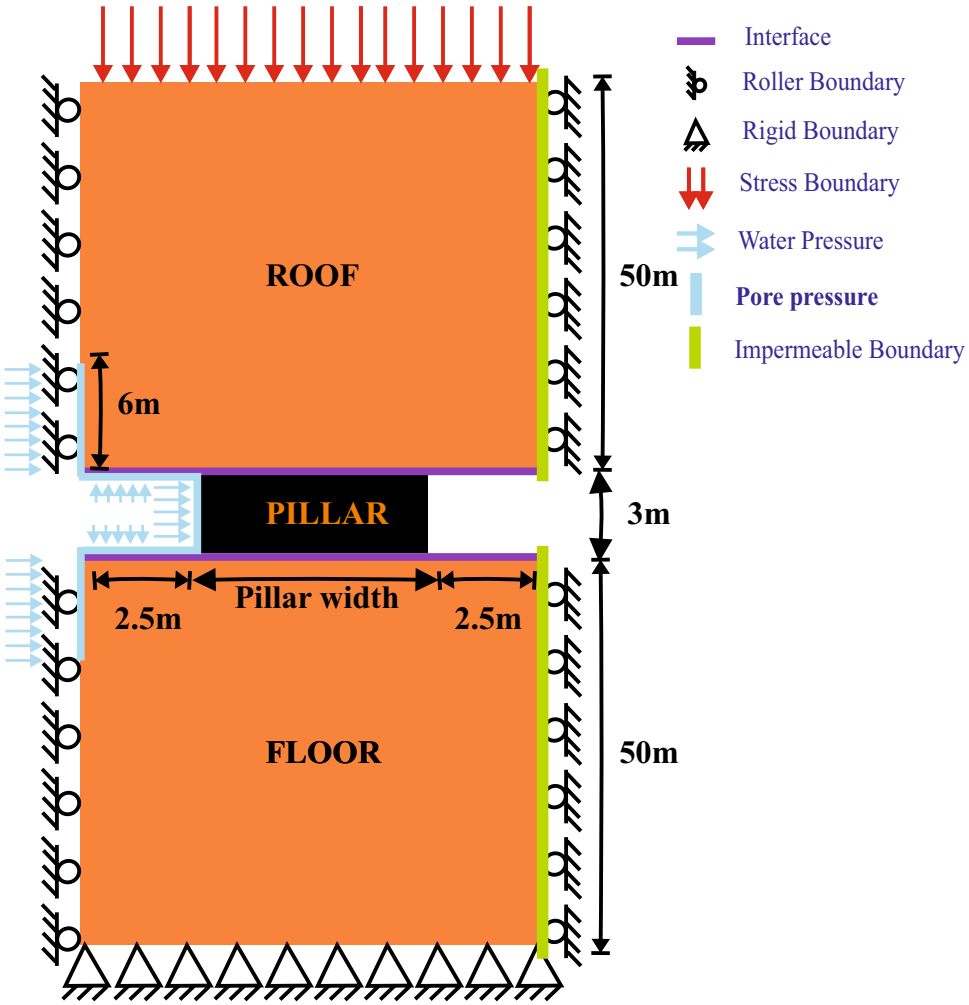

Fig. 2 Model geometry with mechanical and hydraulic boundary conditions

Table 3 Numerical modeling data for parametric study

Rock Type	Density, Kg/m^3			Elastic Modulus, GPa			σc, MPa			σt, MPa		
	Hard	Average	Soft	Hard	Average	Soft	Hard	Average	Soft	Hard	Average	Soft
Roof, floor	2373	2212	1879	13.37	8.50	3.01	20.92	11.68	4.01	2.39	1.22	0.39
Coal	1440	1392	1240	2.4	2.00	1.4	6.32	3.87	2.04	0.71	0.35	0.04

Table 4 Interface properties used in the models

Property	Value	Comment
Normal and shear Stiffness, GPa/m	$10 \times \frac{\left(B+\frac{4}{3}G\right)}{\Delta z_{min}}$	Δz_{min} is the minimum zone size along the interface. The bulk and shear moduli should be of the softer material along the interface (ITASCA 2011)
Cohesion, MPa	0	The presence of water washes away the infill material (Lönnies 2017)
Tensile strength, MPa	0	
Friction angle, °	14	It can vary between 5–25° (ITASCA 2011)
Dilation angle, °	5	

the Stiff Material Testing System (MTS 2022) to obtain their post-failure behavior. A constant rate of loading was applied at 0.005 mm/sec. The test results (Fig. 3b) confirmed the findings reported by Das (1986).

The w/h ratio in the laboratory test samples basically represents the diameter/length ratio of cylindrical samples. Theoretical as well as field experience has confirmed that the w/h ratio of the pillar has a critical role in defining its failure strength and post-failure behavior. Therefore, the mechanical behavior of different samples was simulated to develop the capability to model the post-failure behavior of pillars as designed in the field.

The post-failure behavior, such as peak and residual strength, and the post-failure modulus of the coal material depend on the strain-softening parameters and the zone size of the discretized elements. Hence, the model parameters were calibrated to establish the relationships for estimating the drop rate and the residual cohesion and friction angle values to simulate the observed laboratory behavior. A parametric study was done to simulate the observed laboratory behavior for various w/h ratio specimens of six Indian coal seams (Table 5). The diameter of the platen was fixed at 56 mm, while the thickness of the upper and lower platens was 18 mm for a sample diameter of 54 mm, following the ISRM Standards (Fairhurst and Hudson 1999). The modeled specimen was placed in the center of the platens to facilitate uniform loading. The stiffness of the interfaces was calculated as shown in Table 4, and the effect of friction was evaluated by a trial and error method. It was noted that the effect of change in the strain softening parameter on the ultimate strength was negligible for minimal end friction. Hence, a friction angle of 0.25° was used for the interface between the coal and steel platens, as suggested by Rashed and Peng (2015).

The methodology shown in Fig. 4 was used to estimate the strain-softening parameters. The parametric study considered a w/h ratio of 2–13.5, a zone size ranging from 0.5 × 0.5 mm to 2 × 2 mm, a cohesion drop rate up to 250 MPa/plastic shear strain, a residual cohesion up to 40% of peak cohesion, a friction drop rate ranging from 100–500°/plastic shear strain, and residual friction up to 90% of the peak friction angle (Fig. 5). The variation in dilation angle was incorporated using a 'FISH' function following the Walton and Diederich (2015) model (Eqs. 10–14).

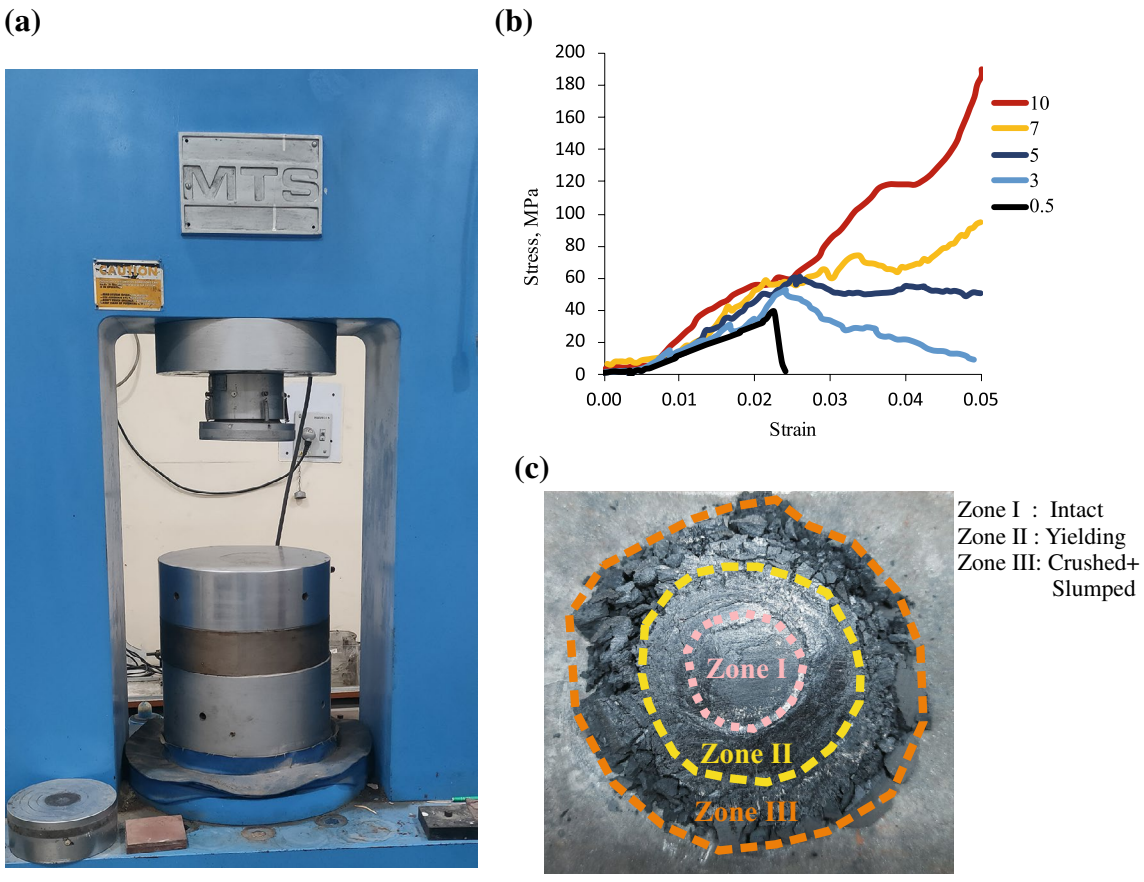

Fig. 3 **a** Material Testing System (MTS) at IIT (BHU), Varanasi **b** Laboratory observed stress–strain behavior of coal samples for a w/h ratio of 0.5–10 **c** zones identified on the top end surface of a coal sample of w/h = 10

Table 5 Properties of a few coal seams in Indian coalfields (Das 1986)

Seam	Elastic Modulus, GPa	Shear Modulus, GPa	Bulk Modulus, GPa	UCS, Mpa	Tensile strength, MPa	Cohesion, MPa	Friction angle, °
Jambad	2.40	0.96	1.60	40.30	2.69	7.15	51
Kargali	4.00	1.60	2.67	31.00	2.07	8.08	35
Kenda	2.70	1.08	1.80	47.48	3.17	10.34	43
Singhpur	4.87	1.95	3.25	37.40	2.49	7.95	44
Uchitdih	1.82	0.73	1.21	20.00	1.33	4.15	45
XII	2.46	0.98	1.64	19.50	1.30	3.95	46

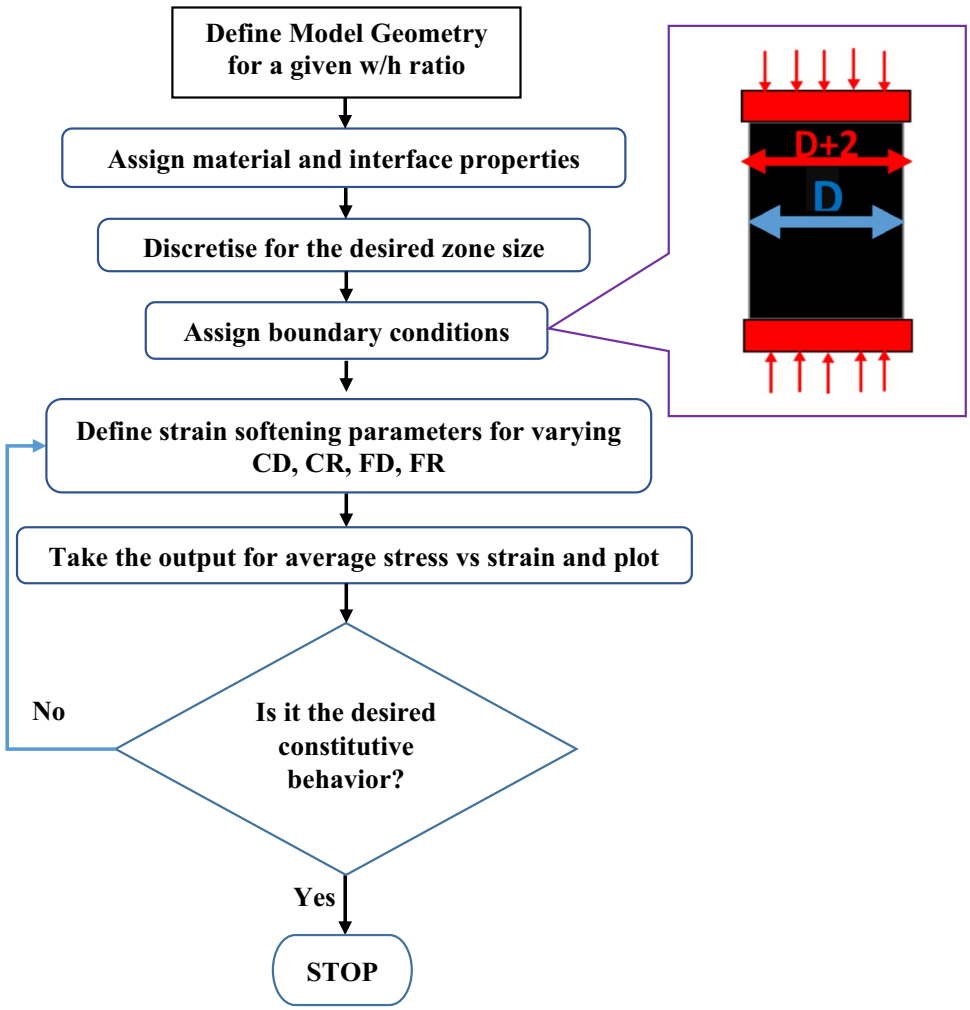

Fig. 4 Methodology of estimating the best-fit strain softening rule

$$\left(\sigma_3,\gamma^p\right)=\begin{cases}\dfrac{\alpha\gamma^p\varphi_{peak}}{e^{\left(\frac{\alpha-1}{\alpha}\right)}\gamma_m} & when \quad \gamma^p<e^{\left(\frac{\alpha-1}{\alpha}\right)}\gamma_m\\ \varphi_{peak}\left(\alpha ln\left(\dfrac{\gamma^p}{\gamma_m}\right)+1\right) & when \quad e^{\left(\frac{\alpha-1}{\alpha}\right)}\gamma_m\le\gamma^p<\gamma_m\\ \varphi_{peak}e^{\left(\frac{-(\gamma^p-\gamma_m)}{\gamma^*}\right)} & when \quad \gamma^p\ge\gamma_m\end{cases} \tag{10}$$

$$\alpha=\alpha_0+\alpha'\sigma_3 \tag{11}$$

$$\gamma^*=\begin{cases}\gamma_0 & when \quad \sigma_3=0\\ \gamma^* & when \quad \sigma_3\neq 0\end{cases} \tag{12}$$

where:

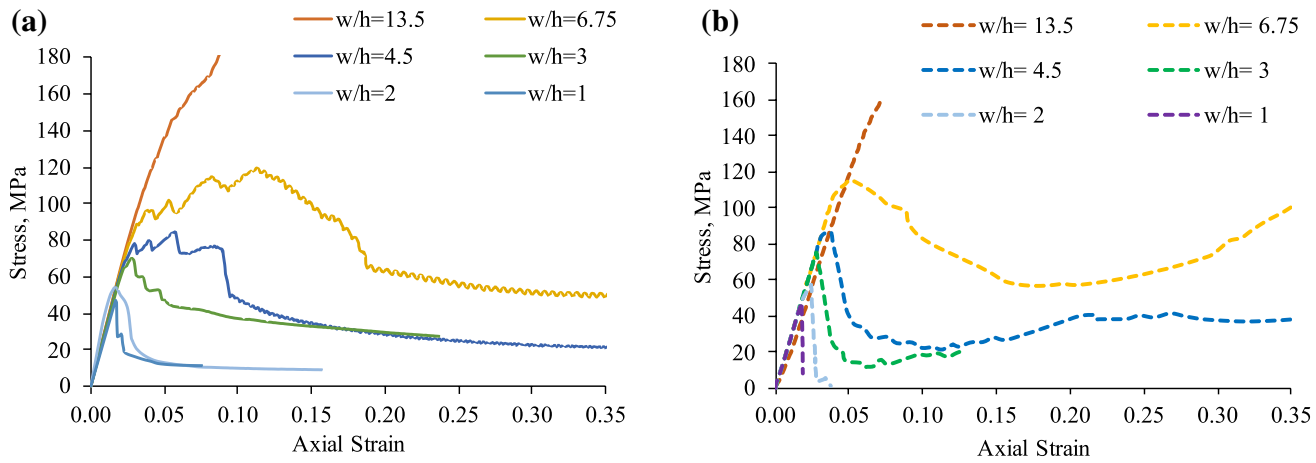

Fig. 5 A comparative plot of **a** model and **b** laboratory-tested stress–strain behavior of different coal specimens of Kenda Seam

$$\varphi_{peak}(\sigma_3) = \frac{\varnothing_{peak}}{1 + log_{10}\left(\frac{UCS}{\sigma_3+0.1}\right)} \tag{13}$$

and

$$\gamma^p = \in_1^p - \in_3^p \tag{14}$$

where α_0 is the curvature of the pre-mobilization in the absence of any confinement, $\alpha\prime$ is the pre-mobilization curvature changes as a function of σ_3, $\varnothing_{peak}$ is the maximum angle of internal friction in °, UCS is the uniaxial compressive strength in MPa, σ_3 is the horizontal stress in MPa, γ_m is the plastic shear strain at peak dilation, γ_0 is the post-mobilization decay rate of the dilation angle in the absence of any confinement, γ^* is the post-mobilization decay rate in the dilation angle for non-zero confinement, $\in_1^p$ is increase in the major principal plastic strain, and $\in_3^p$ is the increase in the minor principal plastic strain.

Thousands of models were run to match their results with the laboratory findings reported by Das (1986) using a trial-and-error iterative approach. The best-fit findings were subsequently used to establish the statistical models (Eqs. 15–18) for cohesion and friction drop and the residual cohesion and friction values as a function of compressive strength, friction angle, modulus of elasticity of coal, dimension of the specimen, and zone size.

$$CD = \frac{22.49\sigma_c^{0.63}E^{1.42}Z_s^{0.60}}{\left(\frac{w}{h}\right)^{0.06}\phi^{0.65}}, \quad R^2 = 0.76 \tag{15}$$

$$CR = \begin{cases} 0 & \forall w/h \le 2 \\ 11.43 \bullet \ln\left(\frac{w}{h}\right) - 7.33 & \forall w/h > 2, R^2 = 0.96 \end{cases} \tag{16}$$

$$FD = \left\{ \begin{array}{ll} 100 & \forall w/h \le 2 \\ 300 or 500 & \forall 2 < w/h < 6.75 \\ 500 & \forall w/h \ge 6.75 \end{array} \right\} \tag{17}$$

$$FR = 50 \tag{18}$$

where CD is the rate of cohesion drop in MPa/plastic shear strain, FD is the rate of friction drop in °/plastic shear strain, CR is residual cohesion in the percentage of peak cohesion, FR is residual friction in terms of the percentage of peak friction angle, σ_c is the compressive strength in MPa, E is the modulus of elasticity in GPa, Z_s is the zone size in m, w and h are the effective width and height of the sample in m, and ϕ is the peak friction angle in degrees.

The hydraulic boundary conditions were prescribed after attaining the post-development mechanical equilibrium. The left-hand side of the pillar formed after excavation was demarcated as a reservoir and the other side as an active mine working. The saturated boundary condition and pore pressure equivalent to the water head were applied on the reservoir side vertical and horizontal edges formed within the excavated region and up to 6 m below and above the water barrier pillar on the vertical boundary of the model. It considered a zone of influence twice the height of the pillar in the roof as well as the floor during long-term hydro-mechanical interaction of water with the surrounding rock mass. The study considers a laminar flow following the Darcy rule through the pillar as the interstice dimensions in rocks are minimal and is subjected to considerable normal and confining stresses.

Results

Three distinct zones, viz. intact or elastic, yielding, and slumped (including the crushed zone) exist in an adequately-sized barrier pillar. These zones are distinguished as per the nature and quantum of deformation induced inside the pillar due to the redistribution of the stresses. The plot of induced permeability in the modelled pillar (Fig. 6a) also showed a similar distribution pattern. The ratio of induced permeability to in situ permeability was plotted for different depth, width, and material strength of pillar. The trends were symmetric about the vertical axis passing through the center of the pillar. Zone-I (intact zone) was characterized by an induced permeability to in situ permeability ratio of one, while Zone-II (yielding zone) developed a maximum induced permeability ratio of 1.05–1.4 in soft rock and 1.02–1.15 in hard rock conditions for pillar sizes ranging between 30–70 m at cover depths of 100–350 m (Table 6). The permeability ratio for zone III (slumped zone) was significantly greater than the upper limit observed in Zone-II. The rate of water seepage also increased with the increasingly induced permeability in the damaged zone (slumped zone + yielding zone). The build-up of the induced permeability in the damaged zone was smoother in the soft rock (Fig. 6b) but was irregular in the hard rock condition (Fig. 6c). However, the model did not indicate any significant change in the seepage rate for a given pillar width with changes in the strength of the rock material. A sharp change in the induced permeability was observed beyond the critical pillar width when no intact zone was left in the pillar in both cases (Fig. 6b, c). The pillar was left with only two high permeability zones, and the rate of change of the induced permeability increased exponentially for the reduced width. A high seepage rate was observed, equivalent to the induced permeability for the given water head (Table 6).

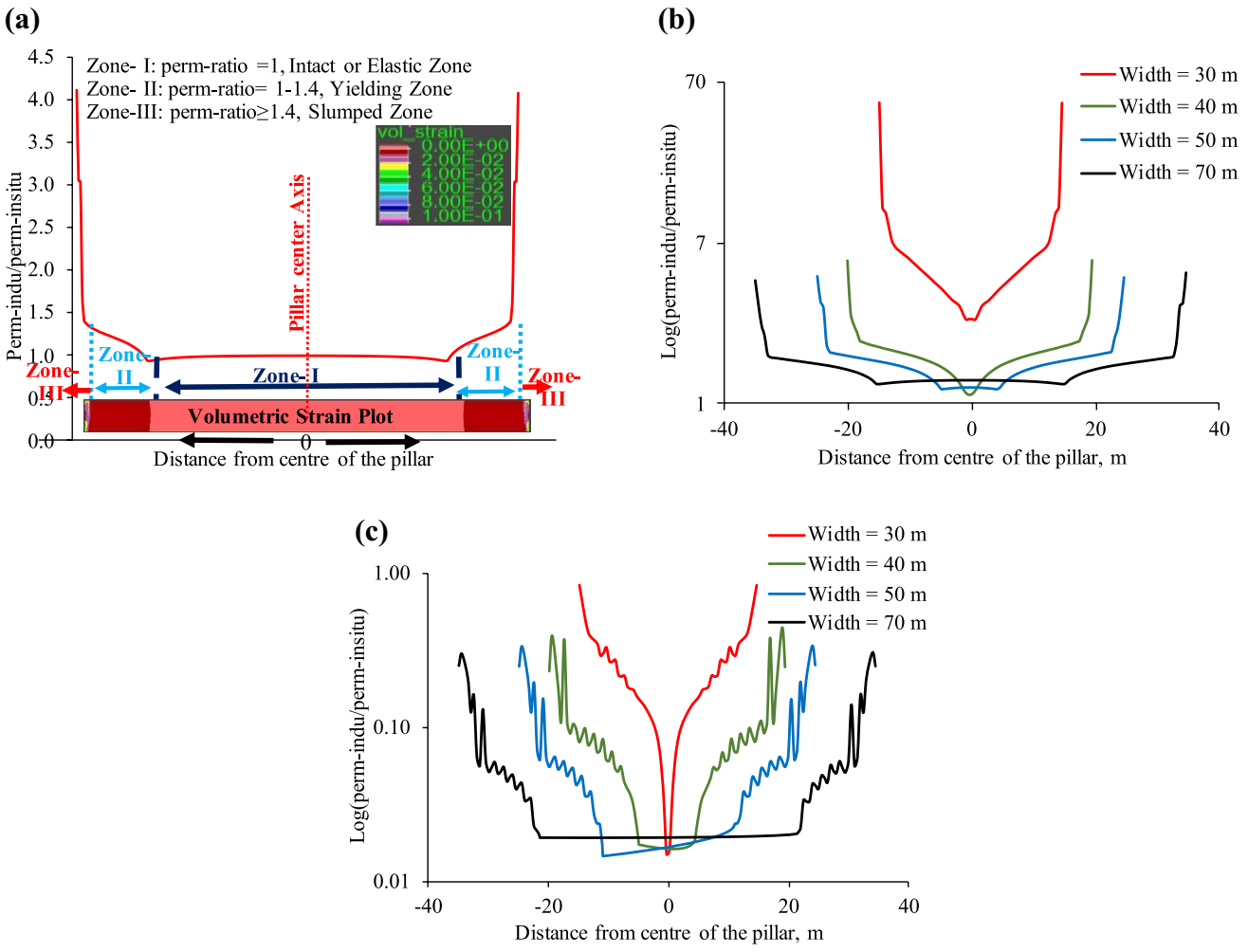

Fig. 6 **a** Zone-wise variation in induced permeability in soft rock formation for 30 m wide pillar at a cover depth of 350 m, **b** and **c** induced permeability profile for a pillar width of 30–70 m at a cover depth of 350 m under soft and hard rock conditions, respectively

Table 6 Seepage and ZoPVS with the variation of depth, width, and strength of the rock formation

Depth, m	Width, m	Soft rock formation		Hard rock formation		Induced Permeability ratio for Zone II	
		ZoPVS, %	Q, L/s/km	ZoPVS, %	Q, L/s/km	Soft	Hard
100	30	51	375	37	372	1–1.05	1–1.02
100	40	39	288	28	286		
100	50	32	235	23	233		
100	70	24	172	17	171		
250	30	100	985	80	976	1–1.3	1–1.03
250	40	85	757	61	750		
250	50	69	617	50	611		
250	70	51	453	37	449		
350	30	100	1386	87	1373	1–1.4	1–1.15
350	40	92	1065	67	1055		
350	50	75	868	54	860		
350	70	55	637	40	632		

Figure 7 shows the contour of induced pore pressure and water seepage for a barrier pillar of 30 m width at 350 m depth against a water head of 350 m, considering the highest permeability of coal and nether rock formations. The pore pressure front decreased while moving from the reservoir side to the active mine working side (Fig. 7a) due to the concentration of load. A high volumetric strain was observed at the pillar corners, which decreased inward (Fig. 7b). Hence, high seepage was observed from the corners of the pillar system flow regime on the active working side.

Table 7 shows the variation in the zone of positive volumetric strain (ZoPVS, %) and the seepage through the pillar system with changes in the width of the PWBP for the hard rock condition at a cover depth of 250 m. The water head was 75% of the cover depth, and the permeability of the pillar system was 8.12×10^{-10} m^2/Pa·s. The ZoPVS was calculated as the % of the number of zones having a positive volumetric strain with respect to the total number of zones in the barrier pillar. The change in the seepage rate was calculated as the ratio of the change in seepage with respect to the change in the width of the barrier pillar. An exponential change in seepage was observed as the barrier pillar width was reduced from 30 to 20 m. The limiting width was 25 m, corresponding to 95% of the ZoPVS. Observation of the full range of the parametric study also revealed that a ZoPVS of 95% indicated an exponential increase in the seepage rate. Hence, a ZoPVS of 95% was identified as an indicator of piping failure in protective water barrier pillars, irrespective of the geo-mining conditions. This corresponded to ≈80–85% of the ZoF.

Table 8 shows the comparative results of water seepage through the 60 m wide barrier pillar mandated by the Coal Mine Regulation of India (DGMS 2017), along with the limiting width for piping failure at a cover depth of 100–350 m, soft to hard strata conditions, and water head ranging from 25–100% of the cover depth. No significant change in seepage was observed with variation in strength. The study also indicated that the size of the PWBP need not be the same to avoid a piping failure for all cover depths. A pillar width of 11–15 m was sufficient to prevent piping failure at the shallow cover depth of 100 m, while a pillar width of 25–36 m was required at a moderate depth of 250 m and 28–39 m width at the high cover depth of 350 m to meet this requirement in soft to hard strata. Actively limiting the maximum water head to 25% of the cover depth can help meet the controlled flow requirement in active mine workings. This would enable a meaningful reduction in the mandatory limit of minimum pillar width and facilitate improved extraction of minerals that are permanently locked at present because of the excessively conservative design provisions. In cases where active control of the maximum water head is not practical, a higher pumping facility and an optimal barrier size can be opted to deal with the situation on a sustainable basis.

Development of the Governing Equations

Percentage of the Zone of Positive Volumetric Strain

An empirical relationship (Eq. 19) was established for estimating the ZoPVS in the PWBP. The results of 63 models were analysed to establish the relationship using seven independent variables: pillar width, cover depth, compressive strength of coal, modulus of elasticity of coal and roof/floor, and the extraction ratio.

(a)

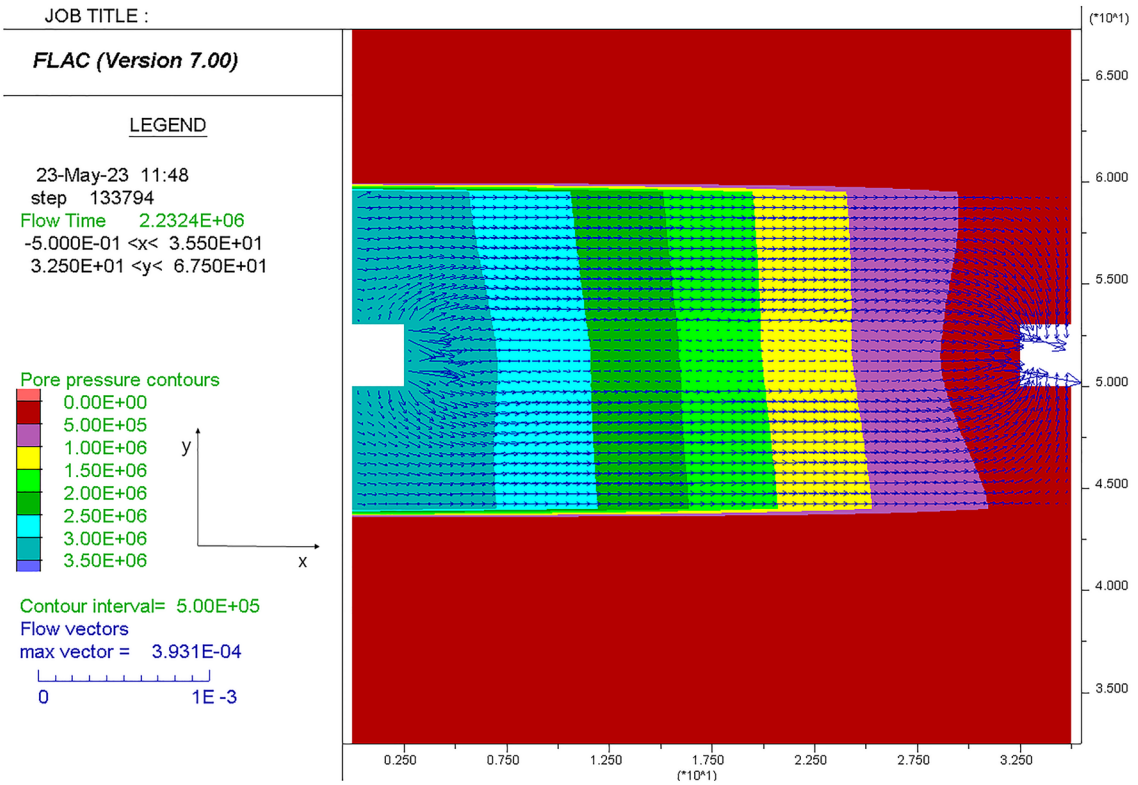
JOB TITLE :
FLAC (Version 7.00)
LEGEND
23-May-23 11:48
step 133794
Flow Time 2.2324E+06
-5.000E-01 <x< 3.550E+01
3.250E+01 <y< 6.750E+01
Pore pressure contours
0.00E+00
5.00E+05
1.00E+06
1.50E+06
2.00E+06
2.50E+06
3.00E+06
3.50E+06
Contour interval= 5.00E+05
Flow vectors
max vector = 3.931E-04
0
1E -3
y
x
(*10^1)
6.500
6.000
5.500
5.000
4.500
4.000
3.500
0.250
0.750
1.250
1.750
2.250
2.750
3.250
(*10^1)

(b)

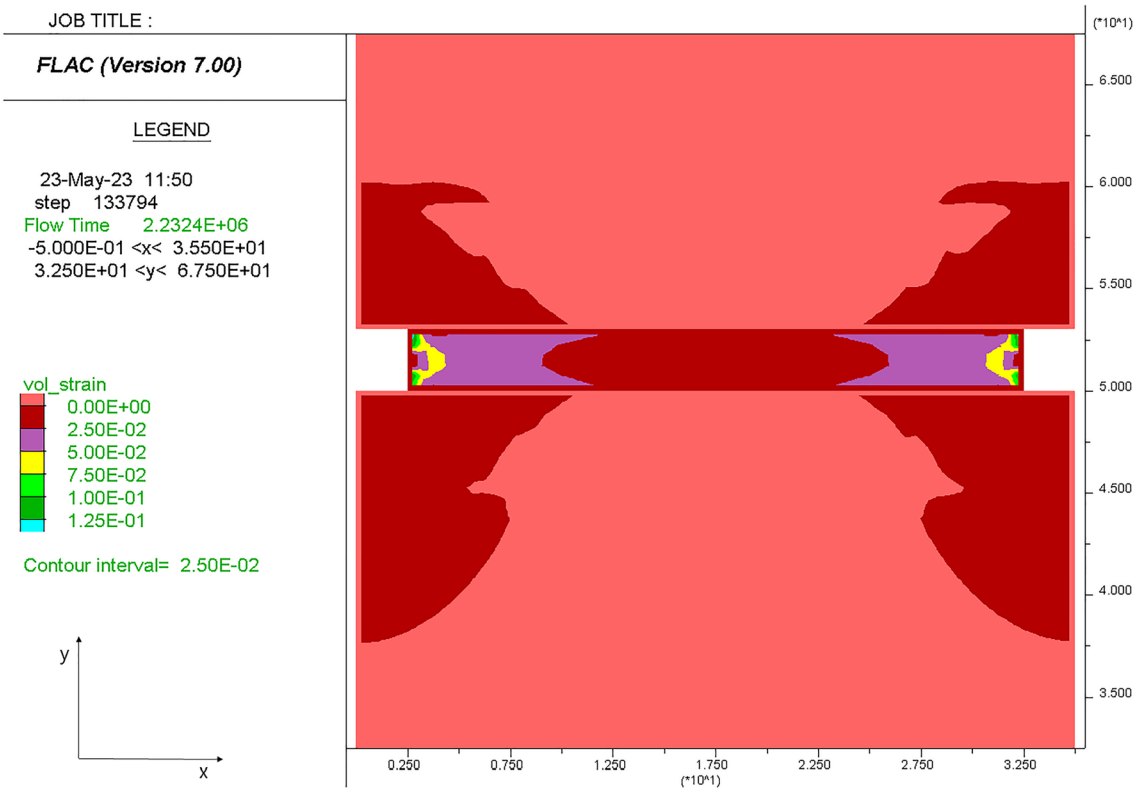
JOB TITLE :
FLAC (Version 7.00)
LEGEND
23-May-23 11:50
step 133794
Flow Time 2.2324E+06
-5.000E-01 <x< 3.550E+01
3.250E+01 <y< 6.750E+01
vol_strain
0.00E+00
2.50E-02
5.00E-02
7.50E-02
1.00E-01
1.25E-01
Contour interval= 2.50E-02
y
x
(*10^1)
6.500
6.000
5.500
5.000
4.500
4.000
3.500
0.250
0.750
1.250
1.750
2.250
2.750
3.250
(*10^1)

◂**Fig. 7** **a** Distribution of pore pressure and seepage **b** distribution of volumetric strain in a 30 m wide barrier pillar against a water head of 350 m and a cover depth of 350 m. (the dimensions along the x and y axes are in meters, and the seepage velocity is in m/s)

$$ZoPVS = \frac{0.04\left(\frac{E_i}{E_c}\right)^{0.27} D^{2.94} e^{0.07}}{\sigma_{hi}^{4.01}\sigma_c^{0.64} w^{0.85}} \quad R^2 = 0.96 \tag{19}$$

where ZoPVS is the zone of positive volumetric strain in %, E_i is the modulus of elasticity of roof/floor in GPa, E_c is the modulus of elasticity of coal in GPa, D is the depth of the workings in m, e is the extraction ratio, σ_{hi} is the weighted average mean horizontal stress in MPa, σ_c is the compressive strength of coal in MPa, and w is the pillar width in m.

Seepage Through Different Geotechnical Flow Regimes

Hundreds of coupled models were run to establish the steady-state total seepage in each flow regime for different conditions. A multivariate statistical regression analysis was conducted to establish the relationship between the seepage through the barrier pillar and the independent influencing parameters. The independent parameters included the: cover depth, compressive and tensile strengths of the pillar system, modulus of elasticity of the coal, roof, and floor strata, mean in-situ horizontal stress of the pillar system, pillar width, extraction ratio, and permeability of the rock matrix. Equations 20–25 describe the relationships developed for estimating seepage for different flow regimes.

I. Flow through the pillar only

$$Q = \frac{0.01k_P\left(\frac{\sigma_c}{\sigma_T}\right)^{1.11}\left(\frac{E_i}{E_c}\right)^{0.17} D^{0.30} e^{0.01} H^{0.99}}{\sigma_{hi}^{0.38} w^{1.05}} \quad R^2 = 0.996 \tag{20}$$

II. Flow through the roof only

$$Q = \frac{0.04k_R\left(\frac{\sigma_c}{\sigma_T}\right)^{0.73}\left(\frac{E_i}{E_c}\right)^{0.11} D^{0.14} e^{0.01} H^{1.03}}{\sigma_{hi}^{0.19} w^{0.92}} \quad R^2 = 0.998 \tag{21}$$

III. Flow through the floor only

$$Q = \frac{0.20k_F\left(\frac{\sigma_c}{\sigma_T}\right)^{0.03}\left(\frac{E_i}{E_c}\right)^{0.01} D^{0.09} e^{0.02} H^{1.03}}{\sigma_{hi}^{0.15} w^{0.85}} \quad R^2 = 0.999 \tag{22}$$

IV. Flow through pillar and roof

$$Q = \frac{0.32k_{PR}^{0.99}\left(\frac{\sigma_c}{\sigma_T}\right)^{0.26}\left(\frac{E_i}{E_c}\right)^{0.03} D^{0.16} e^{0.01} H}{\sigma_{hi}^{0.23} w^{0.93}} \quad R^2 = 0.998 \tag{23}$$

V. Flow through pillar and floor

$$Q = \frac{0.10k_{PF}^{0.98}\left(\frac{\sigma_c}{\sigma_T}\right)^{0.52}\left(\frac{E_i}{E_c}\right)^{0.08} D^{0.23} e^{0.02} H^{1.03}}{\sigma_{hi}^{0.37} w^{0.91}} \quad R^2 = 0.993 \tag{24}$$

VI. Flow through pillar system (Roof, Pillar, and Floor)

$$Q = \frac{0.48k_{RPF}\left(\frac{\sigma_c}{\sigma_T}\right)^{0.21}\left(\frac{E_i}{E_c}\right)^{0.03} D^{0.18} e^{0.02} H^{1.01}}{\sigma_{hi}^{0.26} w^{0.90}} \quad R^2 = 0.999 \tag{25}$$

where Q is the seepage through the PWBP in GPM/km (1 GPM = 0.063 L/s), w is the pillar width in m, e is the extraction ratio, σ_{hi} is the weighted average mean horizontal stress in MPa, σ_c is the rock-mass compressive strength of coal in MPa, σ_T is the rock mass tensile strength of coal in MPa, E_i is the modulus of elasticity of roof/floor in GPa, E_c is the modulus of elasticity of coal in GPa, D is the cover depth of the working in m, H is the water head in m, k_P is the permeability of the pillar in millidarcy (mD) (1 mD=9.90×10^{-13} m^2/Pa·s), k_R is the permeability of the roof in mD, k_F is the permeability of the floor in mD, k_{PR} is the weighted average permeability of the pillar and roof in mD, k_{PF} is the weighted average permeability of the pillar and floor in mD, and k_{RPF} is the weighted average permeability of roof, pillar, and roof in mD.

Field Validation

Model validation was done for two case studies pertaining to the Satgram Incline and Lower Kenda coal mines located in Paschim Burdhaman District of West Bengal, India, under the command area of Eastern Coalfields Limited. Figure 8 shows the location of these mines in the zoomed view of the geographical map. Site-specific data, including the joint mine plan, leasehold area, mining history, borehole sections, average rainfall, the makeup of the mine water, rate of dewatering, and seepage through the pillar, were collected for these mines, along with other site-specific and experience-based observations.

The Satgram Incline Mine

The Satgram Incline mine of Satgram Area is working the Dishergarh coal seam, which is almost completely developed; depillaring is ongoing at present. The leasehold area

Table 7 ZoPVS and seepage in hard rock condition at a depth of 250 m, water head of 75% of depth

S. No. (i)	Barrier width, m (X_i)	ZoPVS, %	Seepage through pillar system, L/s/km (Y_i)	Seepage / pillar width $(Y_{(i+1)}-Y_i)/ (X_i-X_{(i+1)})$
1	150	18	167	
2	140	20	178	1.1
3	130	21	190	1.3
4	120	23	205	1.4
5	110	24	222	1.7
6	100	27	242	2.0
7	90	29	266	2.5
8	80	33	297	3.0
9	70	37	336	3.9
10	60	43	387	5.1
11	50	50	457	7.0
12	40	61	561	10.4
13	30	80	730	16.9
14	25	94	863	26.5
15	20	100	1058	39.1

Table 8 Analysis for seepage characteristics of pillar system

Depth, m	Condition for width	Pillar Width, m		Seepage for Head in % of depth, L/s/km							
				25		50		75		100	
		Hard	Soft	Hard	Soft	Hard	Soft	Hard	Soft	Hard	Soft
100	Width for piping failure	11	15	229	174	462	351	696	529	930	707
	Width as per CMR'17	60	60	49	49	98	99	147	149	197	199
250	Width for piping failure	25	36	285	206	573	414	863	624	1154	834
	Width as per CMR'17	60	60	128	129	257	259	387	390	517	522
350	Width for piping failure	28	39	361	269	727	541	1095	816	1464	1090
	Width as per CMR'17	60	60	180	181	362	365	545	549	728	735

of the mine is 2,300,000 m^2 with a total mined area of 703,800 m^2. The cover depth of the mine ranges from 65 to 130 m and is 84.5 m near the PWBP. The mine was developed with a pillar size of 30 × 30 m (center-center) and a gallery width of 4.5 m. The extraction height of the mine is 2–2.5 m, with exposure of carbonaceous shale laminations in the immediate roof. The mine shares its boundary with the Jamuria A-B Pit Colliery of the Sripur Area, which is abandoned and waterlogged. The minimum width of the inter-mine barrier is 60 m, extending up to 650 m in length (Fig. 9). Table 9 shows the lithology and the associated rock properties used in this study. In the absence of site-specific data, the permeability of the coal was reckoned as 9.90×10^{-11} m^2/Pa·s, while it was 9.90×10^{-10} m^2/Pa·s for the intercalation of shale and sandstone in the immediate roof and floor based on analysis of the literature and engineering judgement. The water seepage of 23 L/s (367.2 GPM) was estimated using Eq. 2 from the overburden (Table 10).

The 60 m wide PWBP developed a ZoPVS of 15% at a cover depth of 85 m, indicating that the barrier pillar was mechanically stable. Figure 10 shows half of the barrier pillar along with the immediate roof and floor on the active working side, along with the seepage through it. The numerical modeling estimated water seepage of 125 L/s/km (1979 GPM/km) against the statistical estimate of 123 L/s/km (1954 GPM/km) through the barrier pillar at the water head of 84.5 m prevailing in the mine. The contribution of seepage through the floor, pillar, and roof in the total seepage was 38, 54, and 33 L/s/km, respectively.

Lower Kenda Colliery.

The Lower Kenda Colliery is located in the Kenda Area of Eastern Coalfields Limited and was started in 1928. The mine has been developed and depillared in different sections. The leasehold area of 6,353,300 m^2 has been worked in three seams, R-VII, R-VI, and R-V, at cover depths of 57–170 m. The present work is ongoing in the R-V seam,

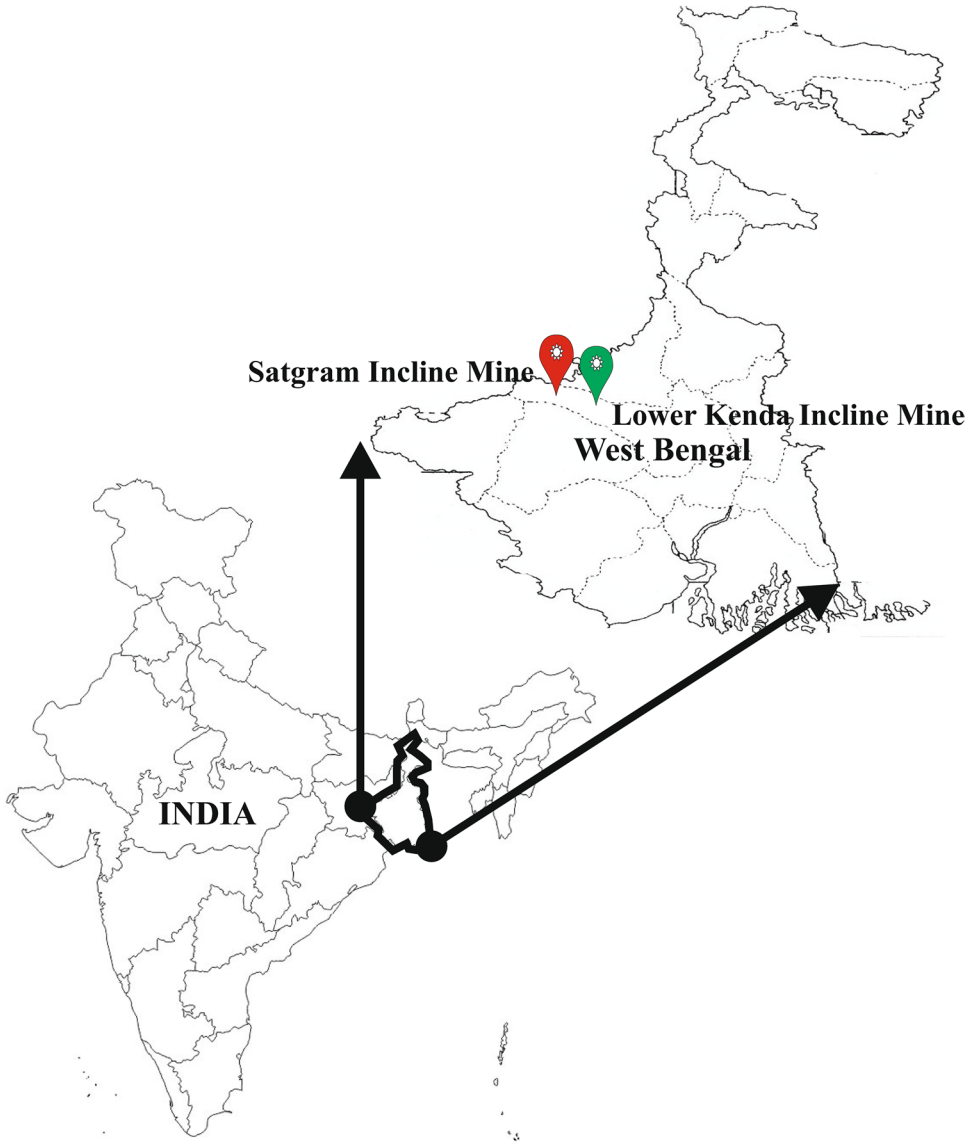

Fig. 8 Geographical Location of Lower Kenda and Satgram Incline Mine in Raniganj Coalfields, India

which is 5.79 m thick. The mine was developed using pillars of 30 × 30 m size (center-center) and extraction height and gallery width of 3 m and 4.8 m, respectively. A portion (2.5 m) of the coal was left in the roof during development. A cover depth of 134.5 m was recorded from the borehole section near the PWBP (Fig. 11). The RMR of the immediate roof is 51–56. The mine shares adjoins the abandoned and inundated Haripur Colliery in the same area, which creates water seepage. The pumping rate of the mine in the normal season is 151 L/s (2,400 GPM), which increases to 227 L/s (3,600 GPM) during the rainy season. The minimum inter-mine barrier thickness is 30 m, which is extended to 700 m along its length (Fig. 11). The rock mass data for this mine is shown in Table 11. The permeability values for the coal, and immediate roof and floor were determined as in the previous case. The water seepage through the overburden for the given conditions (Table 12) was estimated as 108.7 L/s (1,724.3 GPM).

Figure 12 shows the magnified view of half of the barrier pillar along with the immediate roof and floor towards the active mine working side. The 2.5 m of coal left in the roof forms the immediate roof of the workings with an extraction height of 3 m, whereas the floor was composed of fine-grained sandstone. The observed ZoPVS was 34%, which confirmed its mechanical stability. The observed seepage through the floor, pillar, and roof were 123, 139, and 38 L/s/km, respectively. The model observed seepage was 300 L/s/km (4,754 GPM/km), while the statistically estimated seepage was 296 L/s/km (4,693 GPM/km) for a maximum water head of 134.5 m.

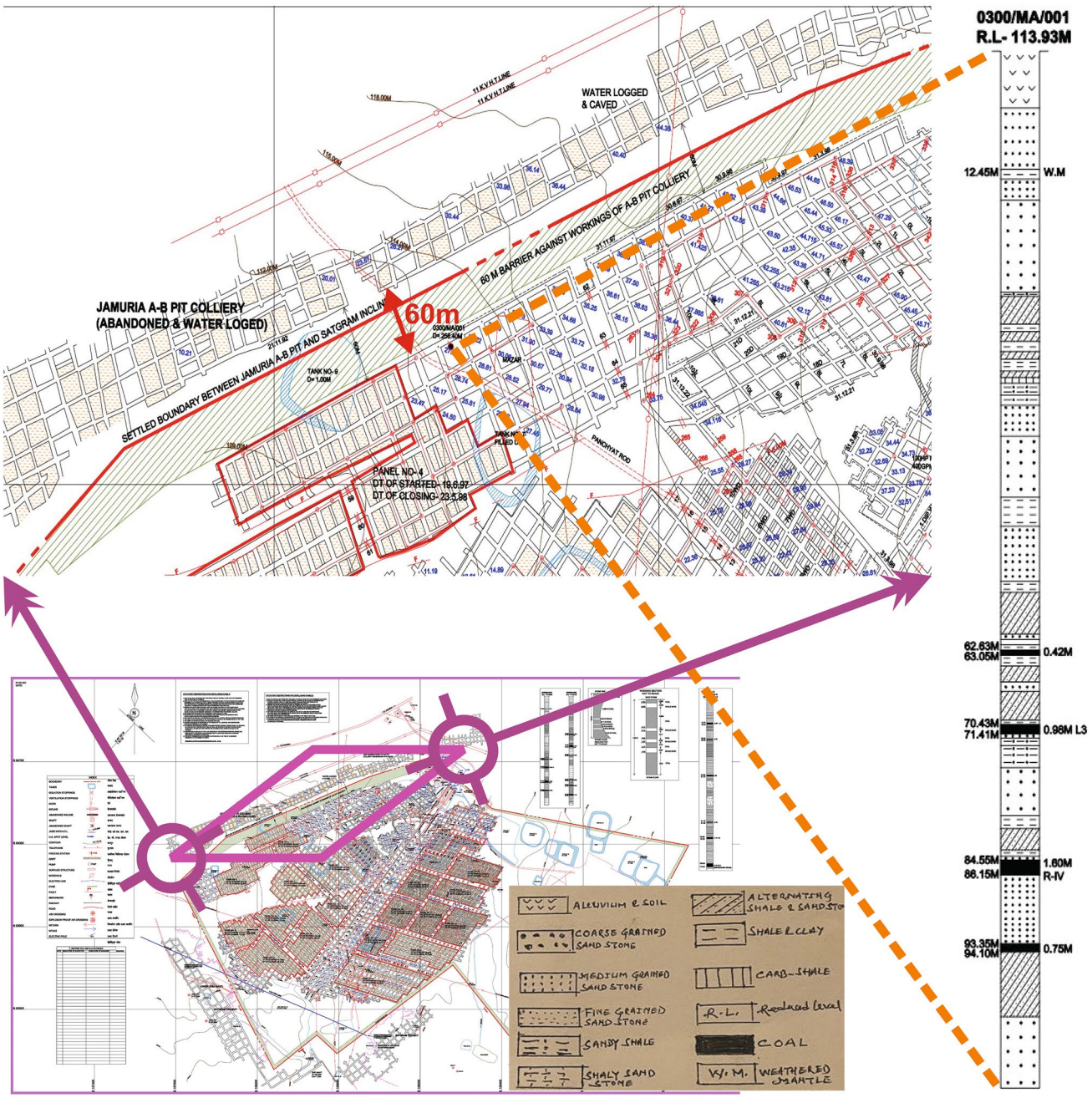

Fig. 9 Joint mine plan showing the minimum barrier thickness of 60m between the Satgram Incline working and abandoned waterlogged AB Pit Mine

Discussion and Conclusions

Optimal design of the PWBP is necessary to protect active mine workings from accidental mine inundation. The adequacy of a PWBP is decided by its mechanical as well as hydraulic performance against a given loading and level of competency. The prevailing approach of PWBP design is extremely conservative, causing a huge loss of coal. Field data pertaining to the existing design of PWBPs show significant deviations from the minimum size as mandated under regulatory provisions in the Indian geo-mining conditions. This extensive study was carried out to provide an in-depth understanding of the performance of such pillars and develop a suitable approach for their optimal design.

The results of the laboratory studies indicated brittle-type post-failure behavior of pillars for a w/h ratio of 0.5–3, strain-softening behavior for a w/h ratio of 4.5–9, and strain-hardening behavior for a w/h ratio of 13.5. This was

Table 9 Rock mass data for the numerical modeling of Satgram Incline mine working

Structure	Thickness, m	Density, kg/m^3	Shear mod., GPa	Bulk mod., GPa	Tensile strength MPa	Cohesion MPa	Friction angle, °	Dilation angle, °
Alluvium & Soil	6	1775	0.27	0.45	0.06	0.10	40	5
Intercalation	56.5	2335	4.86	8.10	1.82	3.81	40	5
Coal	0.5	1380	0.74	2.22	0.60	1.91	25	2
Intercalation	7.5	2334	5.37	8.94	1.79	3.56	40	5
Coal	1	1380	0.74	2.22	0.60	1.91	25	2
Shale, Clay	4	2341	4.68	7.80	1.17	2.02	40	5
Medium Grained Sandstone	5.5	2293	4.07	6.79	1.48	3.47	40	5
Intercalation	3.5	2334	5.37	8.94	1.79	3.56	40	5
Coal	2	1380	0.74	2.22	0.60	1.91	25	0
Fine Grained Sandstone	7	2373	5.35	8.92	2.26	4.62	40	5
Coal	1	1380	0.74	2.22	0.60	1.91	25	2
Floor	50	2312	4.59	7.65	1.63	3.51	40	5

Table 10 Estimation of water seepage through overburden in Satgram Incline Mine

Specifics	Values
Leasehold area, m^2	2,300,000
Mineable area, m^2	2,070,000
Mined area, m^2	703,800
Average rainfall, m^3/Annum	4,140,000
Rainfall infiltration factor	0.06
Maximum feasible groundwater quantity, m^3/Annum	730,588.2
Vertical seepage through strata, L/s	23

successfully captured by the strain softening-based modeling approach implemented in this paper. The mobilization of the dilation angle based on plastic shear strain was critical for simulating the expected post-failure behavior of the coal pillar. The statistical models correlated well with the outcome of the numerical modeling. The suggested statistical models for CD, CR, FD, and FR, along with the Walton and Diederich model for the dilation angle, could be used to simulate the strain-softening behavior of coal pillars.

The ZoPVS-based criteria provided an improved evaluation of the mechanical performance of the pillars. Although the state of the stresses and the ZoPVS for a PWBP were not significant for different flow regimes in a given geomining condition, the flow across the pillar increased when the roof and floor were also contributing to the seepage. Since coal is fairly impermeable, it allows only low seepage unless heavily fractured. However, the immediate roof and floor are mainly sandstone, which is typically more permeable than the coal pillar. Distinct zones of deformation were noted along the width of the pillars due to the redistribution of stress surrounding the excavation and hydraulic pressure acting on it. The distribution profile of induced permeability followed a similar trend (Fig. 6). The model did not indicate much change in the seepage rate as the ratio of compressive to tensile strength of the rock material varied from 8 to 10 for the hard and soft conditions of the strata. Long-term seepage through the pillar was expected to modify the permeability and porosity characteristics of the rock as a function of positive volumetric strain, as hypothesized in this study. With reduced resistance and increased seepage until achievement of the steady state condition, the rock matrix of the pillar is expected to absorb a great deal of water, causing a drastic reduction in its effective strength irrespective of its initial strength.

This study did not consider anisotropic permeability in PWBP design. A proactive strain softening approach was used to capture the influence of water on the strength reduction of rock and its resultant effect on induced plastic strain developed during the loading of the pillar in different conditions. Failure of a PWBP was defined as unable to protect an active mine against accidental inundation due to uncontrollable seepage of water from an adjoining inundated mine despite adequate pumping infrastructure. The approach adopted for coupled modelling was intended to ensure that the model outcome of stress–strain behavior and its reflection in terms of the seepage through the pillar is representative of the conditions prevailing in the field. Compliance with this basic requirement has enabled us to ignore anisotropic hydraulic conductivity for this study.

The pillar corners were observed to create greater seepage than other locations on the active side of the workings. These corners were highly stressed and crushed during load redistribution. The associated damage in terms of the volumetric strain was clearly visible. The high volumetric strain at the corners led to a significant increase in induced permeability.

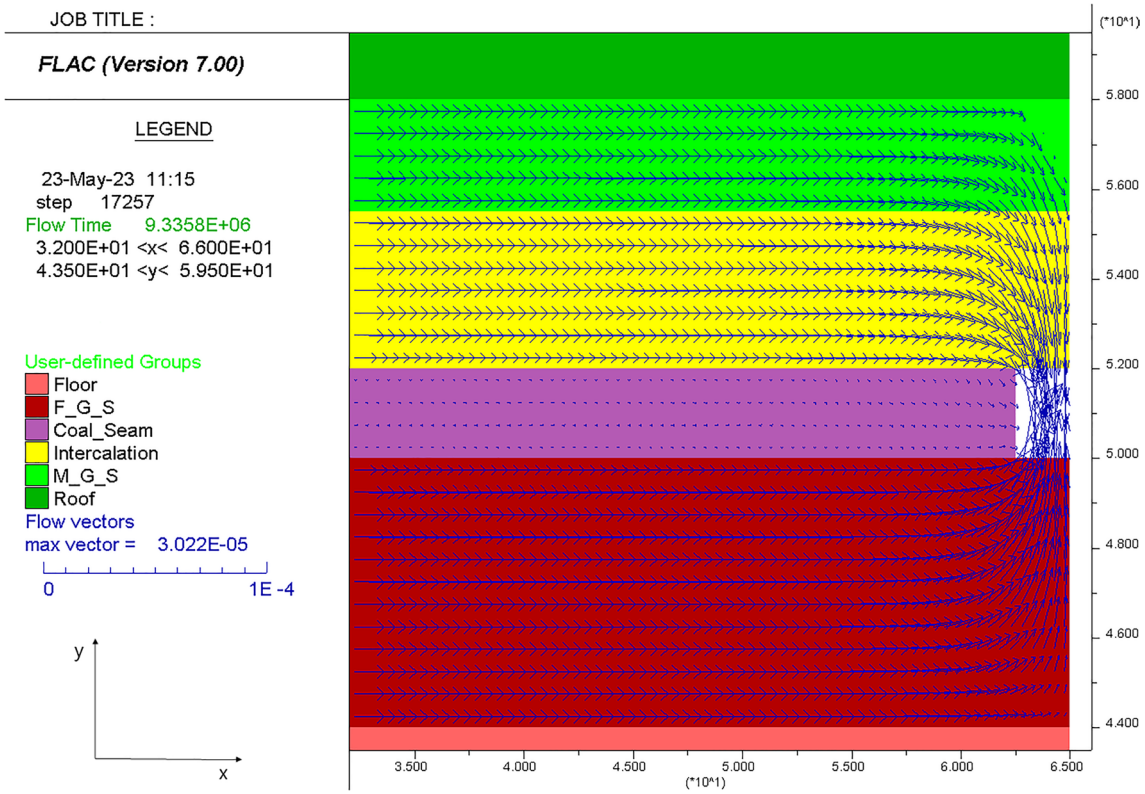

Fig. 10 Flow vectors on the active part of the mine working in Satgram Incline mine (the dimensions along the x and y axes are in meters, and the seepage velocity is in m/sec)

Hence, a high seepage was anticipated from these locations. Also, the seepage from the top corners was greater than from the bottom corners because of the gravitational force.

Based on the seepage observations in several mines and the experience of miners, an approach for the classification of water seepage through PWBPs has been formulated (Table 13). A seepage of 315 L/s/km (5,000 GPM/km) was reckoned as the maximum allowable seepage for the controlled build-up of water that a mine can handle with a reasonable effort.

The performance of a PWBP is governed by its mechanical as well as hydraulic stability. The mechanical stability of the pillar can be assessed in terms of ZoPVS. The statistical model for ZoPVS (Eq. 19) and the steady-state seepage relations for different flow regimes (Eqs. 20–25) correlated well with the results of the hydro-mechanical coupled model. These statistical models were developed using the outcome of the numerical models to provide an easier-to-use tool for assessing the performance of the pillars. The outcome of the statistical model was verified with site-specific field observations and their numerical modelling results. The protective water barrier pillar must adhere to the mechanical stability requirement, quantified in terms of ZoPVS, as a function of pillar width, cover depth, compressive strength of coal, modulus of elasticity of coal, roof/floor, and the extraction ratio. The extent of the pillar having a positive volumetric strain was greatly influenced by the mean in-situ horizontal stress and depth of cover. The uniaxial compressive strength and the pillar width also had a considerable influence. The governing relationship for water seepage was established as a function of the cover depth of the coal seam, compressive and tensile strengths of the pillar system, modulus of elasticity of coal, roof, and floor, mean in-situ horizontal stress in the pillar system, pillar width, extraction ratio, and permeability of the rock matrix. The structural relationship of the seepage rate for different flow regimes indicated the great influence of water head and pillar width and the small influence of extraction ratio on the rate of flow. The strength ratio (σ_c/σ_T) of the strata had the least influence when the seepage was only allowed through the floor (considering the roof and the pillar as impermeable). The maximum influence of the strength ratio was noted when the roof and floor were considered impermeable, and the flow was allowed only through the pillar. The suggested relationship for seepage in different flow regimes could be used in conjunction with the seepage severity classification to assess the hydraulic performance of the PWBP.

Figure 13 shows the plot of ZoPVS and seepage rate with respect to pillar width for the hard rock conditions at a water head of 75% of the cover depth of 250 m. The results are

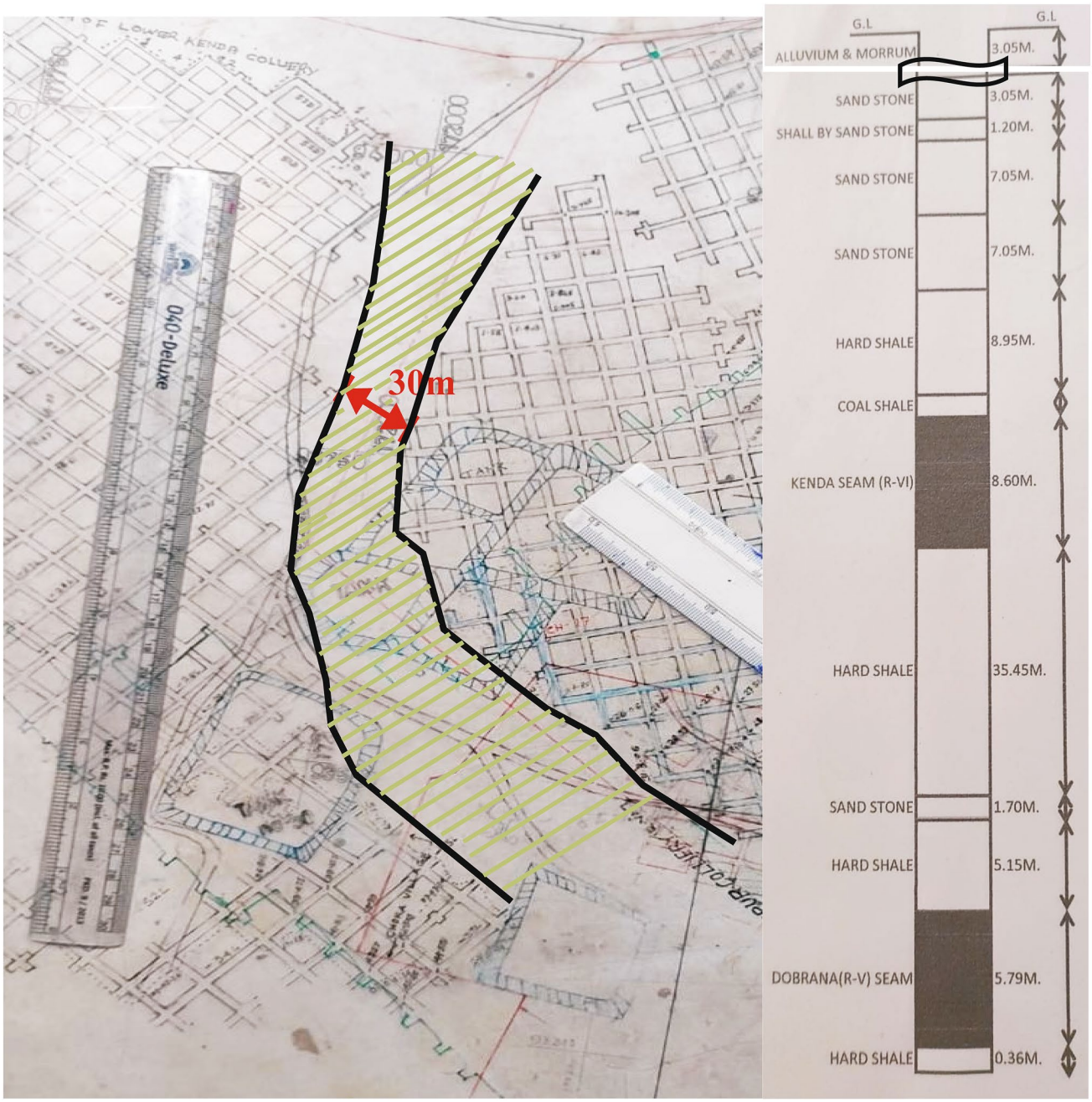

Fig. 11 Joint mine plan showing the minimum barrier thickness of 30m between the Lower Kenda Mine and the abandoned waterlogged working of Haripur Colliery

also compiled in Table 7. The criteria for piping failure and controlled seepage provided a good representation of the rate of change in seepage and ZoPVS. The results of the parametric study also revealed that a ZoPVS of 95% was associated with an exponential increase in the seepage rate. Hence, a ZoPVS of 95% was identified as the indicator of piping failure in PWBP, irrespective of the geo-mining conditions. The pillar width for piping failure and controlled flow were estimated as 25 and 75 m, respectively, for this condition. A maximum ZoPVS of 95% provided an acceptable yardstick for this purpose. A ZoPVS exceeding 95% indicated unstable behavior of the pillar, which is vulnerable to piping failure.

The findings of the study revealed that the width of the pillar should be adjusted based on the depth of the workings and geo-mining conditions (Table 8). A PWBP of 60 m width, as suggested under the regulatory provisions, was revealed to be highly conservative, causing a huge loss of coal at shallow cover depths. This criteria does not account

Table 11 Rock mass data for numerical modeling of Lower Kenda mine working

Structure	Thickness, m	Density, kg/m^3	Shear mod., GPa	Bulk mod., GPa	σt, MPa	Cohesion, MPa	Friction angle, °	Dilation angle, °
Alluvium & Morrum	8.0	1775	0.27	0.45	0.06	0.10	40	5
Fine Grained Sandstone	11.5	2339	4.79	7.98	2.06	4.07	40	5
Coal	8.0	1380	0.74	2.22	0.60	1.91	25	2
Medium Grained Sandstone	58.0	2330	4.62	7.70	1.88	4.08	40	5
Coal	4.5	1380	0.74	2.22	0.60	1.91	25	2
Intercalation	36.5	2349	5.03	8.38	2.02	4.07	40	5
Coarse Grained Sandstone	5.5	2307	3.90	6.51	1.14	2.13	40	5
Coal	5.5	1380	0.74	2.22	0.60	1.91	25	0
Fine Grained Sandstone	4.0	2373	5.35	8.92	2.26	4.62	40	5
Coal	0.5	1380	0.74	2.22	0.60	1.91	25	2
Floor	45.5	2309	3.96	11.87	1.64	3.63	40	5

Table 12 Estimation of water seepage through overburden in Lower Kenda Mine

Specifics	Values
Leasehold area, m^2	6,353,300
Mineable area, m^2	5,717,970
Mined area, m^2	1,143,594
Average rainfall, m^3/Annum	11,435,940
Rainfall infiltration factor	0.06
Maximum feasible groundwater quantity, m^3/Annum	3,430,782
Vertical seepage through strata, L/s	108.7

for the requirement of appropriate pumping arrangements to deal with high seepage through PWBPs at moderate to high cover depths.

Table 14 shows the desired width of the PWBP for controlled seepage in soft and hard rock conditions at cover depths of 100–350 m and a water head of 25–100% of the cover depth. The observations indicate the requirement for a wider barrier pillar for controlled seepage. The pillar width requirement varies from 3.27–4.55 times the critical width for piping failure for the worst possible water head of 100% of the cover depth in these conditions. For controlled seepage at a cover depth of 100 m, a barrier width of 37 m was found to be suitable against the maximum water head of 100 m. However, at cover depths of 250 and 350 m, it is desirable to have effective control of the maximum water head for an optimal pillar width, considering the balance between the cost of excessive water pumping and the value of the coal locked in such barrier pillars. Thus, a barrier width of 50–75 m is recommended for a cover depth of 250 m, with a water head of 50–75% of the cover depth. Similarly, a barrier pillar width of 71 m is recommended at a cover depth of 350 m, for a water head limited to 50% of the cover depth. Controlling the maximum water head is essential to limit seepage in deep workings.

The seepage across the barrier increases drastically for pillar systems with great cover depth and high permeability. Such conditions require elaborate pumping arrangements for uninterrupted operation of the mine. Experience shows that it is always preferable to control the risk at the source. Hence, regular dewatering of the reservoir should be carried out to keep control of the water head against the barrier pillars. As extracting a large volume of mine water is costly, a detailed cost–benefit analysis is required to find the optimal solution considering mineral conservation and the costs of pumping in different geo-mining situations.

The estimation of the critical width for piping failure was based on a static loading condition, which may not prevail in all mines. In the actual field condition, the barrier pillars are subjected to dynamic loading due to ground vibrations. Hence, narrower pillars may undergo sudden failure, causing a disaster, as experienced in the Bagdigi and Chasnallah Collieries (DGMS 2003; Galav et al. 2021). It is extremely important to avoid blasting while working close to a PWBP, if possible, and practice controlled blasting wherever it is unavoidable to avoid the recurrence of such accidents in the future.

The model for the Satgram Incline mine showed greater seepage from the corners of the pillar (Fig. 10), quite similar to what was observed in the field. Closer scrutiny of the joint mine plan revealed that the PWBP was not directly exposed to the water reservoir along part of the total strike length because of the partially developed galleries on the other side of the mine boundary. Of the total length of 650 m of the pillar, galleries were only developed to 450 m, reducing the effective exposure to about 70%. Hence, the field-representative estimate of water seepage through the pillar was reduced to 56 L/s (889 GPM). This corresponds to a total seepage of

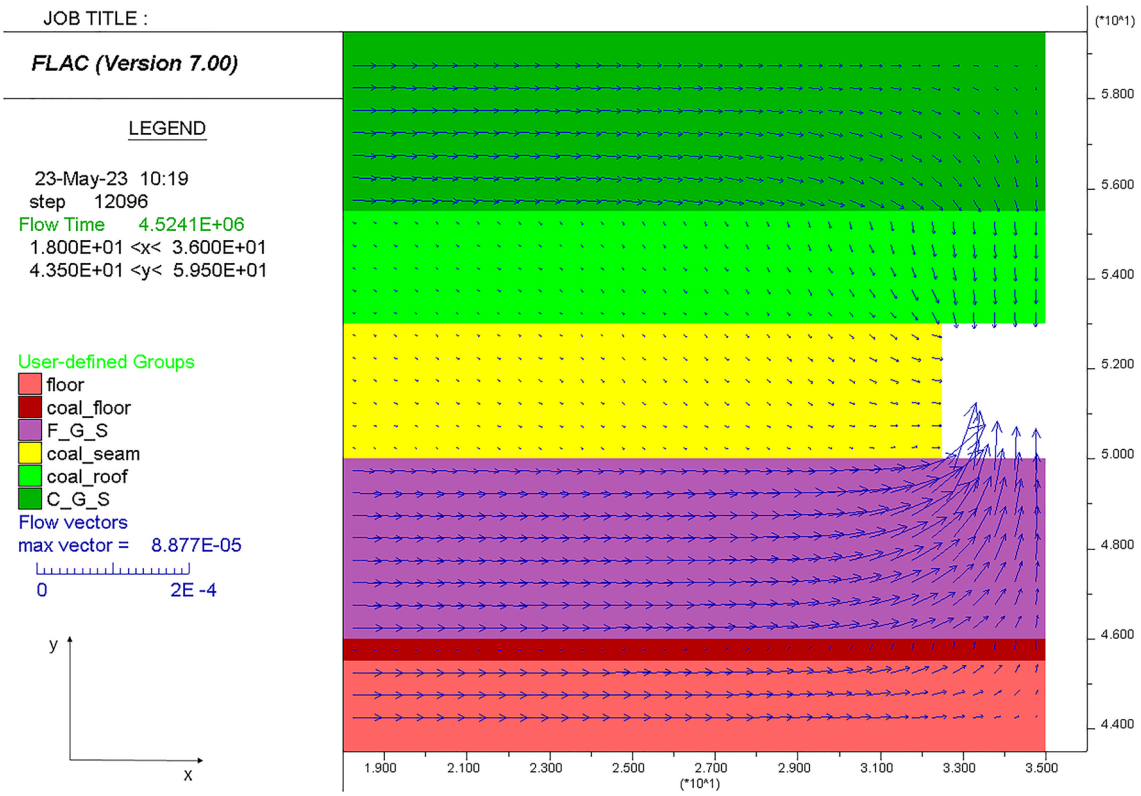

Fig. 12 Seepage velocity trend in the barrier pillar of Lower Kenda mine (the dimensions along the x and y axes are in meters, and the seepage velocity is in m/s)

Table 13 Experience-based classification of the severity of water seepage in Indian Coal Mines

Severity	Seepage Rate, L/s/km (GPM/km)	Remarks
Low	< 95 (1500)	Can be managed easily without any strain on the normal productivity of the mine working
Moderate	95–315 (1500 – 5000)	It is moderately challenging to manage such seepage as it affects the normal production of the mine working by 20–45%
High	> 315 (5000)	Extremely difficult to manage such seepage, which has a considerable adverse effect on mine productivity

79 L/s (1256 GPM), which indicates 'moderate' severity of seepage, as confirmed in the field.

The greater seepage of water through the floor of the barrier pillar in the Lower Kenda mine was also in line with the field observation of large seepage and heaving of the floor. A significant difference in the permeability of the coal in the roof and the sandstone in the floor led to greater seepage from the floor than from the roof. The size of the PWBP at the boundary of the mine ranges from 30–84 m to 50–200 m long segments along the mine boundary. For such variable widths, the effective seepage rate from the barrier pillar was estimated as 125 L/s (1,984 GPM). The resultant total seepage of 234 L/s (3,708 GPM) confirmed the 'high' severity of water seepage, which could only be managed through an elaborate pumping arrangement. Otherwise, there could be considerable operational problems and flooding of the mine. A similar concern was noted in the mine as well.

The models for estimation of the seepage and ZoPVS represented the field observations very closely. Hence, these relationships (Eqs. 19–25) can be used to assess the hydro-mechanical performance of a PWBP in given geo-mining conditions. The findings could also be used to estimate the effective hydraulic conductivity of a pillar system and assess the severity of pumping requirements in mines for existing barrier pillars and the design of PWBPs for new underground workings. This approach will also work as a ready reckoner for the design of PWBPs in Indian geo-mining conditions.

Table 14 Desired width for controlled flow through Pillar System

Depth, m	Width for piping failure, m		Desired width for water head in % of depth, m							
			25		50		75		100	
	Hard	Soft	Hard	Soft	Hard	Soft	Hard	Soft	Hard	Soft
100	11	15	11	15	17	17	27	27	36	37
250	25	36	25	36	48	49	75	76	103	104
350	28	39	33	39	70	71	109	110	150	151

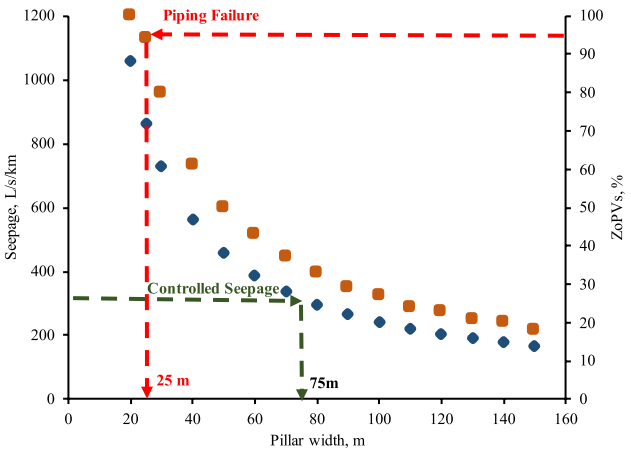

Fig. 13 ZoPVS and seepage for hard rock condition at a depth of 250 m and water head of 75% of cover depth

This study did not consider the effect of geochemical processes on the mechanical and hydraulic stability of the pillar. The research in this area is quite limited, particularly in the context of site-specific coal measure strata, and an appropriate constitutive relationship must still be developed to accommodate the underlying mechanism for the mechanical-hydraulic-chemically coupled phenomenon. Hence, we opted to limit the scope of this research to hydro-mechanical coupling.

Acknowledgements The authors of this paper are grateful for the laboratory and library service rendered by the Indian Institute of Technology (Banaras Hindu University), Varanasi, for this work. The authors express their gratitude to the management of Eastern Coalfields Limited for their assistance. Special thanks to Coal India Limited for funding the study.

References

Chen L, Feng X, Xie W, Zeng W, Zheng Z (2017) Using a fluid–solid coupled numerical simulation to determine a suitable size for barrier pillars when mining shallow coal seams beneath an unconsolidated, confined aquifer. Mine Water Environ 36:67–77. https://doi.org/10.1007/s10230-016-0404-6

Das MN (1986) Influence of width/height ratio on post-failure behaviour of coal. Int J Min Geo-Eng 4:79–87. https://doi.org/10.1007/BF01553759

Dash AK, Bhattacharjee RM, Paul PS (2016) Lessons learnt from Indian inundation disasters: an analysis of case studies. Int J Disaster Risk Reduct 20:93–102. https://doi.org/10.1016/j.ijdrr.2016.10.013

DGMS (2003) Recommendations of Bagdigi Court of inquiry. Accessed 21 Jul 2022, http://www.dgms.net/cir_05_03.pdf

DGMS (2017) The Coal Mines Regulations 2017. https://www.dgms.net/Coal%20Mines%20Regulation%202017.pdf Accessed 21 Jul 2022

Durucan S (1981) An investigation into the stress-permeability relationship of coals and flow patterns around working longwall faces. PhD thesis, Univ of Nottingham

Esterhuizen G, Karacan C (2007) A Methodology for Determining Gob Permeability Distributions and its Application to Reservoir Modeling of Coal Mine Longwalls. Accessed 21 Aug 2022, https://www.cdc.gov/niosh/mining/UserFiles/works/pdfs/amfdg.pdf

Fairhurst CE, Hudson JA (1999) Draft ISRM suggested method for the complete stress-strain curve for intact rock in uniaxial compression. Int J Rock Mech Min Sci Geomech Abstr 36:279–289

Galav A, Singh GSP, Sharma SK (2021) Design and performance of protective water barrier pillars for underground coal mines in India—a review. J Inst Eng India (d) 102:539–547. https://doi.org/10.1007/s40033-021-00286-x

Galav A, Singh GSP, Sharma SK (2022) A numerical modeling approach for assessment of seepage characteristics and performance of protective water barrier pillars in underground coal mines. Min Metall Explor 39:2047–2063. https://doi.org/10.1007/s42461-022-00672-3

Groundwater Estimation Committee (2009) Ground water Resource Estimation Methodology. Report of the ground water resource estimation committee, Ministry of Water Resources, New Delhi, India. Accessed 11 Nov 2022, https://cgwb.gov.in/Documents/GEC97.pdf

ITASCA (2011) FLAC, Fast Lagrangian Analysis of Continua. Itasca Consulting Group Inc, Minneapolis. https://www.itascacg.com/software/FLAC2D. Accessed 20 Oct 2017

Job B (1987) Inrushes at British collieries: 1851 to 1970. Colliery Guardian 235(5):192–9–232–5.

Kendorski FS, Bunnell MD (2007) Design and performance of a longwall coal mine water-barrier pillar. 26th International Conf on Ground Control in Mining, West Virginia Univ, Accessed 20 Oct 2018, https://www.agapito.com/wp-content/uploads/2010/04/Design-and-Performance-of-a-Longwall-Coal-Mine-Water-Barrier-Pillar.pdf

Kesserü Z (1982) Water Barrier Pillars. Proc, 1st IMWA Congress. Accessed 20 Oct 2019, https://www.imwa.info/docs/imwa_1982/IMWA1982_Kesseru_091.pdf

Lönnies V (2017) Evaluation of roof-pillar interface and its effect on pillar stability in mine #101. MS Thesis, Civil Engineering, Luleå Univ of Technology

Luo Y, Peng S, Zhang Y (2001) Simulation of water seepage through and stability of coal mine barrier pillars. Transactions of the North American Manufacturing Research Institute of SME 310:142–147

Meng Z, Shi X, Li G (2016) Deformation, failure and permeability of coal-bearing strata during longwall mining. Eng Geol 208:69–80. https://doi.org/10.1016/j.enggeo.2016.04.029

MTS (2022) Materials Test Systems. Accessed 11 Jul 2022, https://www.mts.com/en/products/www.mts.com

Prusty B, Pal SK, Kumar JH (2015) Study of porosity and permeability of coal and coal measure rocks from Raniganj coalfield of India. Proc, 24th International Mining Congress of Turkey, IMCET, pp 1024–1033

Rashed G, Peng SS (2015) Change of the mode of failure by interface friction and width-to-height ratio of coal specimens. J Rock Mech Geotech Eng 7:256–265. https://doi.org/10.1016/j.jrmge.2015.03.009

Sheorey PR (1994) A theory for in situ stresses in isotropic and transverseley isotropic rock. Int J Rock Mech Min Sci Geomech Abstr 31:23–34. https://doi.org/10.1016/0148-9062(94)92312-4

Singh RN, Atkins AS (1982) Design considerations for mine workings under accumulations of water. Mine Water Environ 1:35–56. https://doi.org/10.1007/BF02504586

Singh GSP (2007) Cavability assessment and support load estimation for longwall workings in India. PhD thesis, I.I.T. (ISM)

Soni AK (2019) Mining of Minerals and Groundwater in India. IntechOpen, London, UK. https://doi.org/10.5772/intechopen.85309.

Walton G, Diederichs MS (2015) A new model for the dilation of brittle rocks based on laboratory compression test data with separate treatment of dilatancy mobilization and decay. Geotech Geol Eng 33:661–679. https://doi.org/10.1007/s10706-015-9849-9

Wang F, Liang N, Li G (2019) Damage and failure evolution mechanism for coal pillar dams affected by water immersion in underground reservoirs. Geofluids 2019:e2985691. https://doi.org/10.1155/2019/2985691

Whittles DN, Lowndes IS, Kingman SW, Yates C, Jobling S (2006) Influence of geotechnical factors on gas flow experienced in a UK longwall coal mine panel. Int J Rock Mech Min Sci 43:369–387. https://doi.org/10.1016/j.ijrmms.2005.07.006

Yang TH, Liu J, Zhu WC, Elsworth D, Tham LG, Tang CA (2007) A coupled flow-stress-damage model for groundwater outbursts from an underlying aquifer into mining excavations. Int J Rock Mech Min Sci 44:87–97. https://doi.org/10.1016/j.ijrmms.2006.04.012

Zhang Y, Li F (2022) Prediction of water inrush from coal seam floors based on the effective barrier thickness. Mine Water Environ 41:168–175. https://doi.org/10.1007/s10230-022-00846-x

Zhang J, Wang J (2006) Coupled behavior of stress and permeability and its engineering applications. Yanshilixue Yu Gongcheng Xuebao/ Chin J Rock Mech Eng 25:1981–1989

Zhao J, Konietzky H, Herbst M, Morgenstern R (2021) Numerical simulation of flooding induced uplift for abandoned coal mines: simulation schemes and parameter sensitivity. Int J Coal Sci Technol 8:1238–1249. https://doi.org/10.1007/s40789-021-00465-x

Zhu H, Zhao X, Guo J, Jin X, An F, Wang Y, Lai X (2015) Coupled flow-stress-damage simulation of deviated-wellbore fracturing in hard-rock. J Nat Gas Eng C:711–724. https://doi.org/10.1016/j.jngse.2015.07.007